IDŐJÁRÁS

QUARTERLY JOURNAL
OF THE HUNGARIAN METEOROLOGICAL SERVICE

CONTENTS

****

http://omsz.met.hu/english/ref/jurido/jurido_en.html

VOL. 108 * NO. 1 * JANUARY - MARCH 2004

IDŐJÁRÁS

Quarterly Journal of the Hungarian Meteorological Service

Editorial Office: P.O. Box 39, H-1675 Budapest, Hungary or
Gilice tér 39, H-1181 Budapest, Hungary
E-mail: prager.t@met.hu or *antal.e@met.hu*
Fax: (36-1) 346-4809

Subscription by

mail: IDŐJÁRÁS, P.O. Box 39, H-1675 Budapest, Hungary
E-mail: prager.t@met.hu or *antal.e@met.hu*; *Fax: (36-1) 346-4809*

IDŐJÁRÁS

Quarterly Journal of the Hungarian Meteorological Service
Vol. 108, No. 1, January–March 2004, pp. 1–10

Radiative forcing tendency due to anthropogenic aerosol particles and greenhouse gases in Hungary

Tivadar Feczkó[1], Ernő Mészáros[1] and Ágnes Molnár[2*]

[1]*University of Veszprém, H-8201 Veszprém, P.O. Box 158, Hungary*
[2]*Air Chemistry Group of the Hungarian Academy of Sciences, H-8201 Veszprém, P.O. Box 158, Hungary; E-mail: amolnar@almos.vein.hu*

(Manuscript received March 14, 2003; in final form November 19, 2003)

Abstract—Radiative forcings of aerosol components and greenhouse gases were studied by a box model in Hungary. Direct climate forcing of aerosol was calculated by using chemical, optical, and meteorological data found in the examined region, while the forcing of greenhouse gases was determined by formulas with global constants and regional concentrations. The climatic effects of these species were compared with their forcings estimated for the beginning of eighties. The climatic effect of ammonium sulfate and carbon dioxide varied significantly during the last two decades. Positive forcing of carbon dioxide increased by 60%, while cooling effect of anthropogenic ammonium sulfate aerosol decreased by 45%. That is, both important trace components in the air helped the warming of regional climate during this period.

Key-words: climate forcing, ammonium sulfate aerosol, carbon dioxide.

1. Introduction

Both aerosol and gaseous components can affect the radiation transfer processes in the atmosphere. Thus, aerosol particles influence *directly* the amount of short-wave radiation reaching the Earth's surface. On the other hand, aerosol can change the climate *indirectly* by modifying microphysical properties of clouds which enhances the cloud reflectivity. This implies that increased concentration of aerosol particles serving as cloud condensation nuclei can change the radiative properties and lifetimes of clouds. Consequently, aerosol produces substantial cooling in the climate system.

* corresponding author

In contrast, greenhouse gases absorb the long-wave radiation emitted by the Earth's surface causing warming of the climate. Estimation of such climatic effects has become an important issue during the last decades, since human activities modify both aerosol and greenhouse gas concentration in the air. We have to take into account in this respect, however, that climate forcing of aerosol particles differs significantly from that of greenhouse gases. This is due to the fact that, while greenhouse gases distribute rather uniformly over the Earth, the concentration of aerosol varies spatially and temporally very much owing to its short atmospheric residence time.

It is well known that radiative forcing of greenhouse gases is generally calculated by global models (*Hansen et al.*, 1988; *WMO*, 1999; *IPCC*, 2001). Similarly, a lot of global climate models have been applied to estimate the direct and indirect radiative forcing of anthropogenic sulfate aerosols (*Charlson et al.*, 1992; *Boucher* and *Lohmann*, 1995; *IPCC*, 1994). The regional behavior of aerosol climate forcing was also studied by high resolution regional climate models (*Ekman*, 2002). In a summarizing work, *Myhre et al.* (2001) show how the anthropogenic and natural climate forcing mechanisms have changed globally from the industrial revolution until present days.

Previously, *Práger* and *Kovács* (1988) worked out a radiative-convective model for average hemispheric circumstances. Using this model by adopting it for Hungary, *Mika et al.* (1993) examined the effect of extra aerosol emission, derived from antropogenic and natural sources, on Hungarian atmospheric radiation balance considering different states of carbon dioxide content. Their radiative-convective model adopted for average atmospheric conditions of Budapest used hypothetical aerosol and gas concentration.

In the present paper the direct aerosol forcing by ammonium sulfate and carbonaceous particles is examined for rural air in Hungary. In addition, the variation of sulfate aerosol forcing estimation is compared with the effect of changes in greenhouse gas concentrations during the last two decades. Aerosol properties and most of the forcing parameters are supposed to be representative for Hungary. The estimation of indirect forcing of aerosol particles will be discussed in a future publication.

2. Data used in the study

2.1 The box model

Both radiative-convective models and box models are used for calculating regional climatic effect of atmospheric compounds. In radiative-convective models the vertical distributions of species are taken into consideration, while to estimate the tropospheric average radiative forcing of aerosol and

greenhouse gases, box models can be applied (*Charlson*, 1991). Considering that data demand of box models is not high, and our results from field measurements can be fitted easily into this model, in our study we applied a simple box model to calculate various forcing mechanisms. The box is imagined as the troposphere over Hungary closed by the tropopause. Since several input data (aerosol extinction, carbon dioxide concentration, incoming solar radiation, etc., see later) refer to K-puszta station or its surroundings, representing Hungarian background air, the simplified box is supposed to describe the air mass over Hungary. It is assumed that the net horizontal transport of measured components is zero, that is, the composition of incoming and outgoing air is chemically equivalent. On the other hand, the air mass is vertically well mixed in the box. For estimating climate forcing, aerosol and greenhouse gas field measurements as well as satellite and meteorological data were used.

2.2 Direct forcing of aerosol

In order to estimate the radiative forcing of aerosol components, their chemical and optical properties were examined simultaneously at K-puszta station, in central Hungary. K-puszta station belongs to GAW and EMEP networks, and the concentrations of different atmospheric constituents (aerosol particles, trace gases) are thought to be characteristic of Hungarian background air. To determine the mass extinction coefficient (the extinction caused by unit aerosol mass) of aerosol components, which is necessary for estimation of direct climate forcing (cf. Appendix), mass concentration of aerosol compounds and extinction coefficient were parallel measured. Aerosol samples were collected by a cascade impactor of two stages separating fine and coarse particles with a cut-off diameter of 1 μm. Ammonium sulfate was analyzed by capillary electroforesis (for more details: *Krivácsy* and *Molnár*, 1998), while total carbon was determined by the catalytic combustion method. It must be noted that only samples taken from morning to evening were analyzed considering the fact that aerosol influences the radiation only in daylight. At the same time scattering and absorption coefficients of fine aerosol particles were monitored at K-puszta station. The scattering coefficient was measured by an integrating nephelometer (M 903, Radiance Research Inc., operating at a wavelength of 550 nm), while the absorption coefficient was observed by a continuous light absorption photometer (model PSAP, Radiance Research Inc., operating at a wavelength of 565 nm).

The direct forcing of aerosol particles caused by the scattering and absorption of light, generally produces negative climatic effect, especially in rural air. This is due to the fact that the great majority of the extinction is

caused by scattering (*Mészáros*, 1999) determined by particles having a size comparable to the wavelength of the light. For this reason only fine particles with diameters between 0.1 μm and 1 μm are taken into account. Our measurements and many other information indicate that under these circumstances the so-called optically active fine aerosol is composed mainly of ammonium sulfate and carbonaceous compounds. Ammonium sulfate and organic species take part in scattering processes exerting cooling influence on climate, while black carbon content of aerosol is mostly responsible for absorption, which results in warming.

Applying the simple box model mentioned, the direct radiative forcing of aerosol in Hungarian rural air was estimated. In this model (for more details see *Feczkó et al.*, 2002) both meteorological parameters and aerosol properties (*Table 1*) were considered, as far as possible by applying regional data.

Table 1. Yearly averaged parameters necessary for calculating the direct climate forcing of aerosol

Parameter	Value
F_0' (W m^{-2})	300
A_c	0.70
R_s	0.21
T_a	0.76
β	0.29

The solar energy change in an air column (called climate forcing) was calculated (see the Appendix) by using the following data: incident solar radiation flux at the top of the atmosphere (F_0'), the fraction of the surface covered by clouds (A_c) – the annual values were gained from satellite observations (ERBE, ScaRaB, METEOSAT). The satellite grid we took into account included K-puszta station, where the aerosol measurements (filter sampling, measurements of scattering and absorption coefficients) were made. The albedo of the underlying Earth's surface (R_s) was derived from the estimation of Hungarian Meteorological Service (*Dávid et al.*, 1990). The fractional transmittance of atmosphere (T_a) above the aerosol layer and the upscattered fraction by aerosol (β) were only considered as global averages.

As mentioned previously, in the model average values are applied, although important seasonal variation could be found in the case of incident solar radiation flux, cloud coverage, and surface albedo (see *Table 2*).

The annual average values were composed of considering seasonal variation of these parameters.

Table 2. Seasonal variation of parameters for calculating direct climate forcing of aerosol

	Spring	Summer	Autumn	Winter
F_0' (W m^{-2})	379	439	231	132
A_c	0.750	0.500	0.625	0.875
R_s	0.177	0.213	0.190	0.267

Multiple regression analysis was used to calculate dry mass scattering coefficients of ammonium sulfate and total carbon as well as the mass absorption coefficient of total carbon from chemical and optical data. The results are presented in *Table 3*. The dependence of mass scattering coefficient on the relative humidity was considered on the basis of results on hygroscopic growth of aerosol particles (*Imre,* 2002).

Table 3. Mass extinction coefficients of main aerosol components

Component	Mass scattering coefficient (m^2 g^{-1})	Mass absorption coefficient (m^2 g^{-1})
Ammonium sulfate	6.1 ± 0.7	–
Total carbon	3.2 ± 0.9	1.0 ± 0.2

2.3 Radiative forcing of greenhouse gases

The effect of well-mixed greenhouse gases on climate in the box can be determined by radiative transfer models (*IPCC*, 1994). These type of calculations generally estimates the climatic effect of greenhouse gases by comparing their concentration to the concentration level before the industrial revolution. We applied the simplified expressions (*Hansen et al.*, 1988; see Appendix) for the calculation of radiative forcing due to CO_2, CH_4, and N_2O, as given in *IPCC* (2001). It should be noted that constants of these expressions refer to global conditions. For the calculation concentrations of gases listed in *Table 4* were used. These concentrations of greenhouse gases were measured in K-puszta and Hegyhátsál, Hungary (the data were kindly provided by *L. Haszpra*).

Table 4. Yearly average abundances of greenhouse gases used in the calculation of climate forcing ([a] estimated over the world, [b] measured in Hungary, *not measured)

Gas	Abundance (year 1750)[a]	Concentration (in 1982)[b]	Concentration (in 2000)[b]
CO_2	278	340	373
CH_4	700	*	1873
N_2O	270	*	315

3. Results and discussion

The main goal of this paper is to examine how the climatic effect of main anthropogenic aerosol components and greenhouse gases has changed during the last two decades in Hungary under rural circumstances. It must be noted that the reliability of forcing estimations for these two classes of atmospheric components are very different. While the uncertainty of calculation of forcing by greenhouse gases can be characterized by a factor of 1.2, the total uncertainty factor of aerosol direct effect is about 2.5 (*Penner et al.*, 1994). Furthermore, the uncertainty of aerosol indirect forcing estimation is probably even more larger. Thus, the comparison of climate forcing of aerosol particles and greenhouse gases directly can be considered with caution owing to the big difference in the uncertainty of forcing estimations.

By taking in mind this discussion, direct climate forcing of main aerosol components was calculated. These calculations show that ammonium sulfate particles cause an important direct aerosol effect on climate in Hungarian rural air (*Table 5*). The yearly average of direct forcing of these particles was found to be $-0.95\ W\ m^{-2}$ *for 2000*. Anthropogenic fraction of ammonium sulfate was determined on the basis of previous sulfur budget calculation for Europe (*Mészáros* and *Várhelyi*, 1982), according to which in 1982 about 10% of sulfate particles originated from sulfur gases emitted by natural sources. Taking into account this sulfate concentration, and assuming that the natural contribution did not change substantially, the anthropogenic climate forcing caused by sulfate particles is equal to $-0.82\ W\ m^{-2}$ *for 2000*. The forcing of ammonium sulfate was also examined for the first half of 1980s, when the sulfur dioxide emission was much stronger than at present as the result of different industrial conditions. According to our estimation, the yearly mean value of anthropogenic ammonium sulfate forcing *in the eighties* was about $-1.45\ W\ m^{-2}$ derived from human activities. In the case of direct climatic effect of carbon, we got smaller value (*Table 5*), it was equal to $-0.6\ W\ m^{-2}$ *in 2000* owing to light scattering, which was decreased by about 15% due to warming

effect by absorption. Unfortunately, we have no reliable estimation about anthropogenic fraction of carbonaceous aerosol for Hungary, and in the lack of previous carbon measurements, we are not able to determine its forcing for the beginning of 1980s.

Table 5. Yearly average direct forcing (W m^{-2}) of ammonium sulfate and total carbon in aerosol (* not determined)

	Ammonium sulfate	**Total carbon**
Natural and anthropogenic (in 2000)	- 0.95	- 0.6
Anthropogenic (in 2000)	- 0.82	*
Anthropogenic (in 1982)	- 1.45	*

According to our estimations for greenhouse gases, the positive climate forcings of carbon dioxide, methane, and nitrous oxide are *1.6, 0.5,* and *0.15 W* m^{-2} (*Table 6*), respectively, *in 2000* relative to the pre-industrial situation. The effect of these gases, which have both natural and human sources, are giving about 85 % of total anthropogenic greenhouse effect (see *IPCC*, 2001). The concentration and consequently climate forcing of carbon dioxide has changed substantially during the last two decades, while the increase of the concentration of the other two greenhouse gases did not cause high effect in this period. The anthropogenic forcing of carbon dioxide was estimated to be *1 W* m^{-2} *at the beginning of 1980s.*

Table 6. Yearly average effect (Wm^{-2}) of greenhouse gases (* global estimation)

	Carbon dioxide	**Methane**	**Nitrous oxide**
Anthropogenic (in 2000)	1.6	0.5	0.15
Anthropogenic (in 1982)	1.0	*0.45	*0.10

We can conclude that the change of climatic effect of ammonium sulfate and carbon dioxide was important in particular during the last two decades in our region. It can also be established that in the time interval *between 1982 and 2000 anthropogenic climatic effect of carbon dioxide increased with a factor of 1.6*, while *for ammonium sulfate it decreased nearly by 45%* owing to the concentration variation of these two components. This means that during the last two decades both atmospheric species contributed to the warming of

local climate in this region. It is noted in this respect that *Myhre et al.* (2001) examined worldwide all natural and anthropogenic forcing mechanisms. They found that radiative forcing between 1945 and 1970 decreased somewhat in spite of the increase in greenhouse gas concentrations. The authors referred explained this primarily by the strong sulfur dioxide emission and its conversion to sulfate aerosol. This global trend surely has been even more significant in the region of central-eastern Europe because of the lack of effective air pollution management. Our results show that the impact of aerosols could have been comparable with the forcing of greenhouse gases in the 80s and probably in the previous decades. On the other hand, significant decline of aerosol forcing has occurred in the last years, therefore, increasing warming effect of greenhouse gases can be expected in the near future. This does not mean, however, that high sulfate concentration would be desirable to compensate climatic impacts of greenhouse gases. Other effects of sulfur emissions like acid rain in regional areas and health damages on local urban scale do exclude such a possibility. Thus, the only solution would be the mitigation of the anthropogenic release of greenhouse gases.

Finally, it is noted that the climate forcing of atmospheric species can be converted to temperature change by a factor, which is called climate sensitivity. This factor is considerably variable in the case of different compounds. Its value depends on the feedback mechanisms considered. If the feedback processes are not taken into account, the climate sensitivity is estimated to be 0.3 K W^{-1} m^2 for both aerosol and greenhouse gases (*Hansen et al.*, 1981; *Charlson et al.*, 1991), which means that 1 W m^{-2} variation in the climate forcing changes the average temperature with 0.3 K.

Acknowledgements—The authors are indebted to *L. Haszpra* from Hungarian Meteorological Service for making available the data sets of carbon dioxide, methane, and nitrous oxide concentrations.

This work was financially supported by the Hungarian Scientific Research Fund (OTKA; project number TS 40903), Hungarian Academy of Sciences (AKP; project number 2000-34 2,5), and National Program on Research and Improvement (NKFP; project number 3/005).

APPENDIX

A. Calculation of direct radiative forcing of aerosol:

due to scattering (*Charlson et al.*, 1991):

$$\Delta F_i^s = -F_0' T_a^2 (1 - A_c) (1 - R_s)^2 \beta \tau_i^s, \quad (1)$$

where $\tau_i^s = \alpha_i^s m_i'$, $\alpha_i^s = \alpha_i^{s,RH} f(RH)$ and $m_i' = m_i H$;

due to absorption (*Haywood* and *Shine*, 1995):

$$\Delta F_i^a = F_0' \, T_a^2 \, (1 - A_c)\omega\beta\tau_i^a \, [(1 - R_s)^2 - 2R_s/\beta(\omega^{-1} - 1)], \tag{2}$$

where $\tau_i^a = \alpha_i^a \, m_i'$; ΔF_i is solar energy change (climate forcing) owing to the scattering/absorption; F_0' is the incident solar radiation flux at the top of the atmosphere; T_a is the fractional transmittance of atmosphere above the aerosol layer; A_c is the fraction of the surface covered by clouds. R_s is the albedo of the underlying Earth's surface; β is the upscattered fraction by the aerosol; τ_i is the aerosol optical depth of ith scattering/absorbing component in aerosol. Further: m_i' is the aerosol column burden of the corresponding component, α_i is the mass scattering/absorption coefficient. $\alpha_i^{s,RH}$ is defined as light-scattering efficiency at a low relative humidity; $f(RH)$ is the relative increase in scattering cross section because of humidity change. The column burden of a given aerosol constituent can be determined as the product of mass concentration (m_i) and the corresponding scale height (H). ω is the single-scattering albedo.

B. Calculation of climate forcing of greenhouse gases

due to CO_2:

$$\Delta F = \alpha \, [g(C) - g(C_0)], \tag{3}$$

where C is CO_2 concentration in ppm, α=3.35 (constant), $g(C)$=ln(1+1.2C+ $0.005C^2+1.4 \times 10^{-6}C^3$);

due to CH_4:

$$\Delta F = \alpha(\sqrt{M} - \sqrt{M_0}) - [f(M, N_0) - f(M_0, N_0)], \tag{4}$$

where M is CH_4 concentration in ppb, $\alpha = 0.036$ (constant);

due to N_2O:

$$\Delta F = \alpha(\sqrt{N} - \sqrt{N_0}) - [(f(M_0, N) - f(M_0, N_0)], \tag{5}$$

where N is N_2O concentration in ppb, $\alpha = 0.12$ (constant),

$$f(M,N) = 0.47 \ln[1 + 2.01 \times 10^{-5}(MN)^{0.75} + 5.31 \times 10^{-15}M(MN)^{1.52}]. \tag{6}$$

References

Boucher, O. and *Lohmann, U.*, 1995: The sulfate-CCN-cloud albedo effect: a sensitivity study with two general-circulation models. *Tellus 47B*, 281-300.

Charlson, R.J., Langner, J., Rodhe, H., Leovy, C.B., and *Warren, S.G.*, 1991: Perturbation of the northern hemisphere radiative balance by backscattering from anthropogenic sulfate aerosols. *Tellus 43AB*, 152-163.

Charlson, R.J., Schwartz, S.E., Hales, J.M., Cess, R.D., Coakley Jr., J.A., Hansen, J.E, and *Hofmann, D.J.*, 1992: Climate forcing by anthropogenic aerosols. *Science 255*, 423-430.

Dávid, A., Takács, O., and *Tiringer, Cs.*, 1990: Distribution of radiative balance over Hungary (in Hungarian). Országos Meteorológiai Szolgálat Kiadványa, No. 66, Budapest.

Ekman, A.M.L., 2002: Small scale patterns of sulfate aerosol climate forcing simulated with a high-resolution regional climate model. *Tellus 54B*, 143-162.

Feczkó, T., Molnár, A., Mészáros, E., and *Major, G.*, 2002: Regional climate forcing of aerosol estimated by a box model for a rural site in Central Europe during summer. *Atmospheric Environment 36*, 4125-4131.

Hansen, J., Johnson, D., Lacis, A., Lebedeff, S., Lee, P., Rind, D., and *Russell, G.*, 1981: Climate impact of increasing atmospheric carbon dioxide. *Science 213*, 957-966.

Hansen, J., Fung, I., Lacis, A. Rind, D., Lebedeff, S., Ruedy, R., Russell, G., and *Stone, P.*, 1988: Global climate changes as forecast by Goddard Institute for Space Studies 3-dimensional model. *J. Geophys. Res. 93*, 9341-9364.

Haywood, J.M. and *Shine, K.P.*, 1995: The effect of anthropogenic sulfate and soot aerosol on the clear sky planetary radiation budget. *Geophys. Res. Lett. 22*, 603-606.

Imre, K., 2002: Study on the higroscopic properties of atmospheric aerosol (in Hungarian). Diplomamunka, Veszprémi Egyetem.

IPCC, 1994: Radiative forcing of climate change. In *Climate Change 1994* (eds.: *J.T. Houghton, L.G. Meira Filho, J. Bruce, H. Lee, B.A. Callander, E. Haites, N. Harris*, and *K. Maskel*). Cambridge University Press, New York.

IPCC, 2001: *Climate Change 2001* (eds.: *J.T. Houghton, Y. Ding, D.J. Griggs, M. Nouger, P.J. van der Linden, X. Dai, K. Maskell*, and *C.A. Johnson*). Cambridge University Press, U.K.

Krivácsy, Z. and *Molnár, A.*, 1998: Size distribution of ions in atmospheric aerosols. *Atmospheric Research 46*, 279-291.

Mészáros, E., 1999: *Fundamentals of Atmospheric Aerosol Chemistry*. Akadémiai Kiadó, Budapest.

Mészáros, E. and *Várhelyi, G.*, 1982: An evaluation of possible effect of anthropogenic sulfate particles on the precipitation ability of clouds over Europe. *Időjárás 86*, 76-81.

Mika, J., Kovács, E., and *Bozó, L.*, 1993: The effect of anthropogenic and natural changes of the atmospheric aerosol content on the radiation balance in the Carpathian basin (in Hungarian). *Beszámolók az 1993-ban végzett tudományos kutatásokról*. Orsz. Meteorológiai Szolgálat, Budapest, 81-89.

Myhre, G., Myhre, A., and *Stordal, F.*, 2001: Historical evolution of radiative forcing of climate. *Atmospheric Environment 35*, 2361-2373.

Penner, J.E., Charlson, R.J., Hales, J.M., Laulainen, N., Leifer, R., Novakov, T., Ogren, J., Radke, L.F., Schwartz, S.E., and *Travis, L.*, 1994: Quantifying and minimizing uncertainty of climate forcing by anthropogenic aerosols. *Bull. Amer. Meteorol. Soc. 75*, 375-400.

Práger, T. and *Kovács, E.*, 1988: Investigation of the climate modifying effects of atmospheric trace gases and aerosol particles by a radiative-convective model (in Hungarian). *Időjárás 92*, 153-162.

WMO, 1999: *Scientific Assessment of Ozone Depletion: 1998*. Global Ozone Research and Monitoring Project. World Meteorological Organization. *Report No. 44*, Geneva, Switzerland.

IDŐJÁRÁS

Quarterly Journal of the Hungarian Meteorological Service
Vol. 108, No. 1, January–March 2004, pp. 11–32

Influence of rain and other meteorological parameters on trace metals in size fractionated particles in polluted urban atmosphere

Antonio J. Fernández Espinosa and **Miguel Ternero Rodríguez**

Department of Analytical Chemistry, Faculty of Chemistry, University of Seville, C. Professor García González s/n, E-41012 Seville, Spain; E-mail: anjose@us.es

(Manuscript received January 3, 2003; in final form June 19, 2003)

Abstract—Relationships between meteorological variables and particles, metals and their size fraction concentrations were determined from samples collected in different climatic situations. Special attention was focused on the effect of rain. Single correlation and multiple regression statistical methods were performed on samples from both rainy and dry days. Coarse particle concentrations diminished linearly when rainfall increased. The metals Fe, V, Ni, Ti, and Mn diminished as well. A substantial concentration effect was produced by the temperature on TSP, Fe, Ti, and Mn concentrations in fine particles. Also, a dispersion effect was produced by the atmospheric pressure on TSP, Mn, Fe, Ti, Ni, and V concentrations in these particles. Besides, there was a dispersion effect by the wind speed on TSP and Cd concentrations. The fine particles and metals between 1.3 and 0.6 micrometers are those best correlated with meteorological parameters. Multiple linear regression was demonstrated to be a powerful tool to explain the particle and metal levels in relation to size distribution and meteorology.

Key-words: size distribution, metals, suspended particles, meteorology, rain, multiple linear regression.

1. Introduction

Suspended atmospheric particles have long lifetimes depending on size and meteorological conditions. Size distribution depends on aerosol sources, but it is also affected by prevailing meteorological conditions. Apart from additional factors, meteorology is the most determinant factor in the removal or dispersion mechanisms of particles and metals in the air. Many studies have

investigated the relationship between meteorological conditions and airborne particles (*Elsom* and *Chandler*, 1978; *Witz* and *Moore*, 1981; *Brooks* and *Salop*, 1983). The latter two used multiple linear regression analyses to relate meteorological parameters to particle and several metal concentrations in the USA, specifically in Los Angeles city and Southeastern Virginia State. We carried out a similar study on particles and lead in Seville (*Melgarejo et al.*, 1986) using single and multiple correlations. The relation between meteorology and particle size distribution has also been the subject of numerous recent and earlier works, such as *Choularton et al.* (1982) in Manchester (UK), *Väkevä et al.* (2000) in Helsinki, and *Despiau et al.* (1996) in a Mediterranean zone of France (Toulon), all of them using single correlations on particles.

To study the nature and magnitude of the meteorology effect on different particle sizes, the first tool is the statistical analysis of correlations (single linear regression). Thus, the first objective is to know, how meteorology influences different sizes, focusing specially on fine particles and toxic metals, which are the most harmful.

As a second important objective, multiple linear regression was considered as a statistical technique for the best information for particle and metal behavior caused by the meteorological parameters.

2. Experimental section

2.1 Measurement sites

This study was done in Seville (38°12'-36°51'N, 4°39'-6°32'W, 10 m a.s.l.), the largest city in southern Spain. Analytical data were obtained from a network of twelve sampling stations already used in our previous works (*Usero et al.*, 1988; *Fernández et al.*, 1999 and 2000). The stations have different traffic intensities and different industrial activities, as well as zones with clean air. Seville is located in the centre of the Guadalquivir Valley, which opens toward the ocean at the base of the triangle that the valley forms.

The city has a warm and dry Mediterranean climate with mean annual temperature of 18°C, rainfall 600 mm, atmospheric pressure 1014 hPa, relative humidity 65%, and wind speed 2 m s^{-1}. Seville is characterized by high temperatures and low wind speeds. Prevalent air currents come from the SW-NE direction. All these data are averaged from the 1961-1990 period (*MMA*, 1997). Predominant winds proceed from the Atlantic Ocean (southwest). Therefore, the situation of this sampling network in Seville

represents the meteorological effects of a Mediterranean zone influenced by the African winds as in other cities of southern Europe.

2.2 Particulate sampling

Atmospheric particles were collected with a high-volume sampler (MCV, Model CAV-A/HF) equipped with a five-stage cascade impactor plus a back-up filter (MCV, Model IC/CAV), which effectively separates the particles. It has the following equivalent cut-off diameters at 50% efficiency (D_p): >10 μm (A particles), 10–4.9 μm (B particles), 4.9–2.7 μm (C particles), 2.7–1.3 μm (D particles), 1.3–0.6 μm (E particles), and <0.6 μm (backup, F particles). For A to E stages, five cut filters (14.2 cm × 14.2 cm) were used, and for the backup filter an uncut filter (20.3 cm × 25.4 cm) was used. Cut and uncut micro-fibre glass filters were purchased from WHATMAN (GF/A).

Granulometric fractions are in accordance with the particle size fraction definitions for health-related sampling (*ISO 7708*, 1995), which defines the fine particles as the fraction below 1 μm. Thus, stages B to F can be associated with PM10 particles, stages D to F with PM2.5 particles, and stages E plus F with PM1 particles (*Fernández et al.*, 2001). The flow rate should be set at the value of 68 $m^3\ h^{-1}$ to get the size separation. The flow rate is calibrated every three months at the Andalusian Reference Laboratory for the Air Quality (LARCA) in Seville.

Care was taken in handling the fibreglass filters in order to avoid contamination problems, and all filter materials and samples were handled within a vertical laminar airflow cabinet, for ensuring air cleanliness standards of class 100 according to Federal Standard 209E.

Forty-one samples were collected in 1996, and three to four samples were usually taken at each sampling station. The sampling time-frame was usually 48 h (about 3264 m^3), and a weekly sample was taken on different days during the following week, so that a possible distorting effect could be avoided.

2.3 Reagents and apparatus

Vertical laminar airflow cabinet with a HEPA filter was from INDELAB (Model IDL-48V). Water bath was from JULABO (Model SW-20C). Centrifuge was from SIGMA (Model 3-15). Standard solutions for metals and acids were from MERCK. Ultra-pure water was from WATERS-MILLIPORE (Milli-Q-grade, Model Plus).

Samples were analyzed for eleven metals (Ca, Fe, Mg, Pb, Cu, Mn, Ti, V, Ni, Co, Cd) by atomic emission spectrometry with inductively coupled plasma (ICP-AES) using a Fisons-ARL 3410 sequential multi-element

instrument. Determinations in the multi-element analysis were done in triplicate for each sample.

2.4 Methodology for the chemical analysis

Samples and blank filters used were stored, treated in a dark room and analyzed individually (A-F) for metal concentrations as in our previous work, *Fernández et al.* (2001). The particle concentration of each stage of suspended particles (FSP) was expressed in μg m^{-3}. The total suspended particles concentration (TSP) was then calculated by summing the particle concentrations of the six fractions (FSP) of each sample.

The metal concentration of each filter (FM) was expressed in ng m^{-3}. The total metal concentration (TM) was then calculated by summing the concentration of the six fractions (FM) of each sample. To differentiate between the different size fractions, these were numbered from 1 to 6, e.g., Fe1 and Fe6 corresponded to the metal Fe collected in stages A and F, respectively.

2.5 Meteorological data

Meteorological data were provided daily by our local service of the National Institute of Meteorology (INM) in Seville. These data correspond to the same periods of each particulate sampling. These values for each sampling correspond to the average hourly data provided throughout the sampling periods. Rainfall values were summed with the hourly data during the sampling period. The meteorological data are represented as follows: precipitation (PP) in mm, ambient temperature (AT) in C, atmospheric pressure (AP) in hPa, wind speed (WS) in m s^{-1}, and wind direction (WD) according to the cardinal points.

In this study we considered the rainy and dry days separately in two matrices, after dividing the "total matrix", which showed some interesting results. The "dry days matrix" was formed by samples collected on non-rainy days, "rainy days matrix" was formed the by samples collected on rainy days.

2.6 Multivariate statistical analyses

On the basis of the results, basic and multivariate statistical analyses were applied to the analytical and meteorological data. For these analyses the STATISTICA (*StatSoft,* 1999) software package was used.

Correlation studies were carried out by applying the simple linear regression (SLR) technique. Because a high correlation coefficient does not necessarily imply linearity, linearity was verified by graphical examination.

Any non-linear case was discarded. The procedure for this not only consisted of choosing the highest correlation coefficients, but also verifying the linearity by observing the linear profile of the points, i.e., the pairs of data x-y. Sometimes, high correlation coefficients do not give a real linearity on a graph, because their line is formed by accumulation of points at the extreme of their linear range and a lone point at the other extreme. In these cases, the correlation coefficients are due to only one sample and not all the experimental data. Outliers are misleading and should therefore be discarded.

Later on, multiple linear regression (MLR) analysis was used to relate the analytical variables, statistically significant in the SLR, to the meteorological parameters, through mathematical multivariate linear functions. For both SLR and MLR, when the correlation coefficient (r) was not sufficiently high, a two-tailed t-test was applied with a 95% confidence level to assess whether $r \neq 0$ was significant. Thus, if the calculated t of the student test was greater than the t tabulated, then r was significantly greater than zero.

From the first calculations of the data, we observed, that in Seville rain is the parameter with the greatest influence on particle and metal levels as opposed to the other parameters. The heterogeneity and distortion factor introduced by the washing effect of the rain makes the conclusions unreliable and justifies the need to treat each situation separately.

The statistical studies took into consideration, firstly, the effect of rain on total suspended particles and total metal concentrations and their size distributions, and secondly, the effect of the remaining meteorological parameters on particle and metal concentrations and their size distributions.

3. Results and discussions

3.1 Meteorological characteristics of the sampling period

During the whole year in 1996, a total of 916.8 mm of rainfall was registered, which represents a considerable increase compared to the previous years (580 mm in 1993, 327 mm in 1994, and 503 mm in 1995). Meteorological parameters recorded only for the sampling period are presented in *Table 1*. The mean rainfall on rainy days was 13.6 mm. Mean wind speed was low, 2.2 m s^{-1}, although it was sufficient to cause the resuspension of soil particles in the air. Depending on maximum values, the effect can reach the dispersion of pollution. It should be noted also, that the temperatures were high. With regard to the frequency of the wind direction, the most common winds were south-westerly or southerly, although, the strongest winds came from the west (*Fig. 1-a*). This was to be expected, because the wind blows up the axis of the Guadalquivir Valley (SW-NE).

Table 1. Mean values of the analytical and meteorological variables corresponding to the sampling period

Variable	Mean	Range	Units	RSD (%)
Meteorological variables				
PP*	13.6	(1.2 - 141.0	mm	167.8
WD	SW	(NW - W)		27.0
WS	2.2	(0.6 - 4.2)	$m\ s^{-1}$	44.3
AT	21.0	(15.3 - 29.8)	°C	20.5
AP	1010.5	(1003.7 - 1018.4)	hPa	0.4
Total and fractionated particle variables				
TSP	78.7	(31.1 - 158.1)	$\mu g\ m^{-3}$	44.0
A	12.1	(3.1 - 27.3)		53.6
B	12.4	(6.6 - 21.1)		33.4
C	4.9	(2.8 - 7.5)		26.9
D	4.0	(2.0 - 6.0)		31.2
E	3.6	(0.8 - 7.1)		46.4
F	41.7	(11.7 - 104.5)		57.0
Total metal variables				
Ca	2956	(345 - 8680)	$ng\ m^{-3}$	81.6
Fe	689	(131 - 1974)		58.3
Mg	366	(200 - 669)		29.2
Pb	97	(15 - 1335)		60.0
Cu	28.0	(8.3 - 74.2)		51.5
Mn	19.8	(4.1 - 141.0)		52.6
Ti	7.4	(1.7 - 16.9)		52.0
V	5.9	(0.6 - 18.0)		76.5
Ni	1.97	(0.47 - 4.31)		58.9
Co	0.56	(0.09 - 2.01)		76.7
Cd	0.44	(0.09 - 4.73)		61.4

*: Mean rainfall on rainy days, RSD: Relative standard deviation in percentage, WD: wind direction

The relationship between wind speed, rainfall, atmospheric pressure, and temperature is an important climatic feature. Thus, the correlation analysis is a good tool, because it shows meteorological behavior, for example, the well known relations between the rain, the decrease of temperature and atmospheric pressure, and the increase of wind speeds. Other results show that mild warm winds come from the south (proceeding from Africa) and slightly less warm winds from the Southwest (the Atlantic Ocean). The coldest winds are also the

strongest, those coming from the west (the Atlantic Ocean crossing Portugal). The highest rainfall values are correlated with south-westerly winds, because the moisture easily penetrates into the valley.

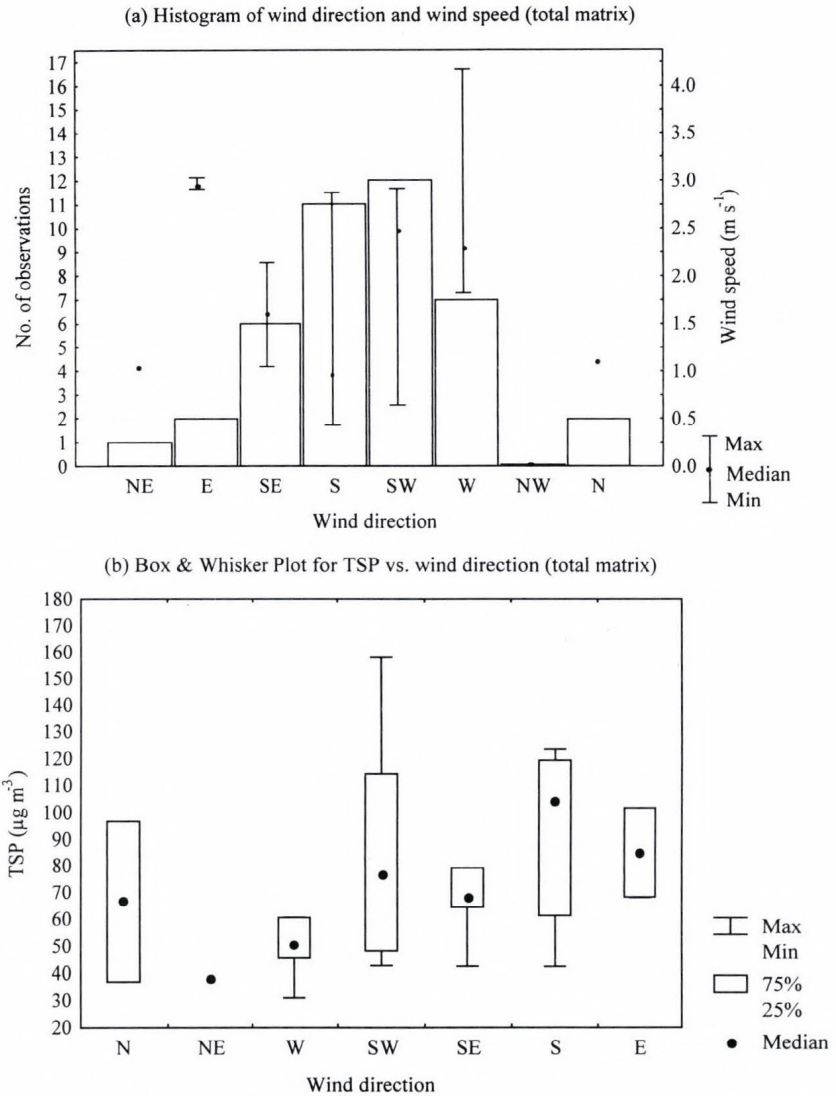

Fig. 1. (*a*) Frequency of wind direction, values of median, maximum, and minimum for wind speeds for all samples. (*b*) Distribution of TSP levels according to the wind directions with values of median, maximum, minimum, and quartiles.

3.2 Basic analytical parameters

In order to know the levels of particles and metals, they are also included in the basic statistics of *Table 1*. The mean value of 78.7 μg m^{-3} for TSP is from 50–150 μg m^{-3}, that would correspond to an "acceptable" air quality according to European directive 1999/30/EC for PM10 particles, but not a "good" air quality (under 50). If the mean value of A particles is subtracted from TSP, the resulting mean value, which would correspond to PM10 particles (sum of B to F stages), is 66.6 μg m^{-3}, still above 50 μg m^{-3}, the final limit value for 24 h. Two samples of TSP exceeding 150 μg m^{-3}, corresponds to a "poor" air quality, although no PM10 value exceeds this value. 23 samples of 41 exceed the limit value for 24 h in PM10 particles, but additionally 16, 12, and 12 samples exceed this value in PM2.5, PM1, and F particles, respectively. The F particles, with D_p<0.6 μm, reaches a maximum value of 104.5 μg m^{-3}. This is relevant, because this size has a high probability of depositing in the alveolar region of the lungs. Remember, that 40% of these 41 samples were collected in rainy days. It is known that the sum of particle concentration of various consecutive filters from a cascade impactor contains errors attributed to a possible accumulation of mass from conversion of gas to particles into the filters. This way, mainly particles lower than 1 μm from this conversion are bound to each stage, increasing the mass of each filter but not changing significantly their percentages regarding the sum. Although this fact exists, it is clear that numerous sum values are much higher than the limit for PM10 particles, even in the sum values corresponding to PM2.5, PM1, and F particles. Because of this effect of accumulation of mass in the sum, we cannot include these PM concentrations as analytical variables in the statistical treatment, except for these comparisons.

In relation to the total metal concentrations, the lead value is five times lower (0.097 ng m^{-3}) than the limit established by the European Community, however, three samples collected near a foundry exceed this limit of 0.5 μg m^{-3}. Therefore, although lower levels of lead are emitted by leaded fuel driven vehicles, high values can be detected locally in the proximity of foundries, for example the maximum value in *Table 1*. These high mean values of particles and low mean values of metals indicate the important influence of the North Western African particles from the Sahara desert.

3.2.1 Total particle content, size distribution, and the effect of rain

In order to study the differences introduced by the rain in particle and metal levels, *Fig. 2* shows the averaged values of concentrations by comparing dry days and rainy days. The great influence of rain is expressed as percentage.

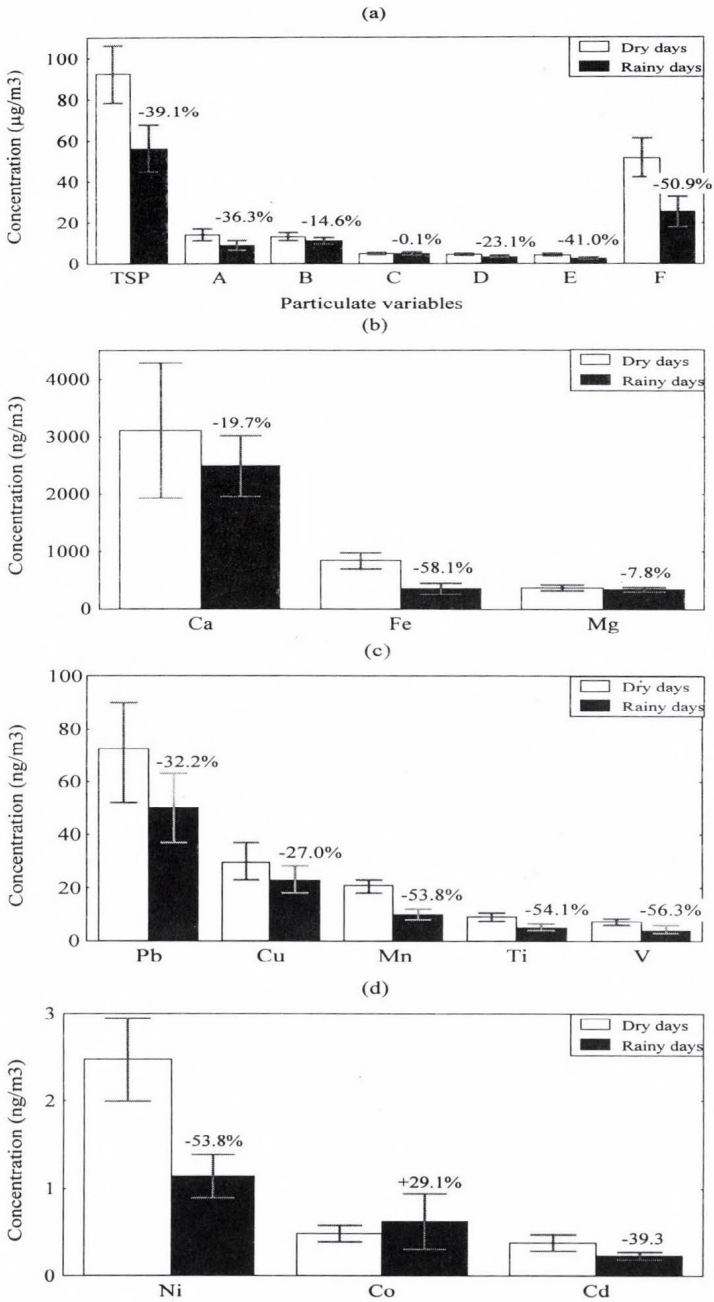

Fig. 2. Averaged values of (*a*) total suspended particles, TSP, and fractionated suspended particles, FSP, and (*b*), (*c*), (*d*) total metal concentration, TM. Effect or rainfall comparing dry days and rainy days.

Table 2. Correlation coefficients (r) for the three matrices of data formed by the meteorological variables, the total suspended particles (TSP), and their size distribution (FSP, A to F), and the metals (TM)

Meteorological variables				Total and fractionated particle variables							Total metal variables										
WS	AT	AP	PP	TSP	A	B	C	D	E	F	Ca	Fe	Mg	Pb	Cu	Mn	Ti	V	Ni	Co	Cd
(a) Total matrix																					
WS	1.00	−0.53	−0.48	0.54	−0.39	−0.43	−0.25	−0.07	−0.37	−0.40	−0.35	−0.13	−0.46	0.01	−0.37	−0.38	−0.47	−0.51	−0.41	−0.50	0.10	−0.56
AT	−0.53	1.00	0.38	−0.51	0.62	0.46	0.35	0.22	0.54	0.61	0.64	−0.30	0.61	0.09	0.37	0.47	0.64	0.59	0.35	0.51	−0.32	0.51
AP	−0.48	0.38	1.00	−0.66	0.12	0.02	−0.16	−0.30	0.00	0.10	0.21	0.01	0.27	−0.10	0.11	0.07	0.28	0.30	0.14	0.20	−0.09	0.16
PP	0.54	−0.51	−0.66	1.00	−0.48	−0.46	−0.31	0.07	−0.24	−0.37	−0.48	−0.05	−0.56	−0.06	−0.20	−0.31	−0.57	−0.54	−0.47	−0.50	0.37	−0.28
(b) Dry days matrix																					
WS	1.00	−0.21	0.03	–	0.03	−0.25	−0.07	0.01	−0.02	0.06	0.13	−0.01	−0.01	0.20	−0.27	−0.36	−0.08	−0.07	−0.12	−0.17	0.06	−0.47
AT	−0.21	1.00	−0.28	–	0.47	0.31	0.28	0.40	0.53	0.50	0.46	−0.48	0.35	0.01	0.29	0.44	0.46	0.32	0.06	0.24	−0.65	0.40
AP	0.03	−0.28	1.00	–	−0.67	−0.62	−0.65	−0.53	−0.62	−0.67	−0.56	−0.15	−0.61	−0.39	−0.21	−0.33	−0.69	−0.57	−0.55	−0.57	0.06	−0.27
(c) Rainy days matrix																					
WS	1.00	−0.13	0.63	0.03	−0.36	−0.24	−0.39	−0.33	−0.46	−0.66	−0.29	−0.37	−0.25	−0.07	−0.08	0.04	0.01	−0.39	−0.22	−0.30	−0.10	−0.43
AT	−0.13	1.00	−0.01	−0.42	0.50	0.45	0.37	−0.16	−0.15	−0.13	0.59	−0.45	0.61	0.01	−0.12	0.18	0.20	0.40	0.60	0.31	0.04	0.04
AP	0.63	−0.01	1.00	−0.24	−0.16	−0.15	−0.37	−0.49	−0.50	−0.41	−0.02	−0.29	0.02	−0.17	−0.29	−0.09	0.37	−0.03	0.15	−0.22	0.11	−0.15
PP	0.03	−0.42	−0.24	1.00	−0.35	−0.61	−0.52	0.16	0.21	0.15	−0.28	0.30	−0.44	0.19	0.15	−0.29	−0.41	−0.24	−0.54	−0.38	0.42	0.07

WS: wind speed, AT: ambient temperature, AP: atmospheric pressure, PP: precipitation

Also, single correlations of particles and metals with meteorological parameters are shown in *Table 2*. This table highlights the positive and negative correlation coefficients that indicate the linear behavior between particle and metal concentrations and meteorological parameters. In *Fig. 2-a*, the decrease in concentration of the fine particles (E particles: - 41%, and mainly F particles: - 51%) is greater than that of coarse particles (A particles: 36%, B particles: 15%). However, in *Table 2-c*, the higher anticorrelation with rainfall can be observed for particles larger than 4.9 μm, mainly the A particles > 10 μm (r = - 0.61); meanwhile, the value for F particles is low (r = - 0.28). This fact seems to be a contradiction, but one observes an easy explanation: the fine particles are those that are eliminated in large proportion (-51 % in *Fig. 2-a*) independently of the quantity of rain (- 0.28 in *Table 2-c*). Meanwhile, the coarse particles are those that respond more linearly to the removal and washing effect of the rain (-0.61 in *Table 2-c*). Thus, fine particles are removed from the atmosphere independently of the amount of rain, whereas elimination of coarse particles is dependent on rainfall values.

On the other hand, in *Table 2-c*, the negative correlation between TSP and rainfall was not as significant as might be expected (r = - 0.35). This fact can be explained by the differences in the correlation coefficients of the different size fractions (from - 0.61 for A particles to + 0.21 for D particles). This is one of the aspects that justifies the importance of studying the particle sizes for meteorological and environmental interpretations.

Regarding the influence of rain on metal contents, the lowest values were observed again for the rainy days (*Fig. 2-b,c,d*, *Table 3*). The percentages for the size fractions of metals can be seen in *Table 3*. In the last file, the highest negative percentages of total concentrations were found for Fe (-58.1%), vanadium (-56.3%), Ni (-53.8%), Ti (-54.1%), and Mn (-53.4%), but on the contrary, high positive percentages of cobalt (+29.1%) were found. The higher values are for fine particles, except for vanadium (-67.0%) and calcium (-51.8%), which are for coarse particles. The high percentages found in rainy samples correspond to the majority of size fractions of cobalt, mainly the E particles, and several fractions of magnesium and cadmium.

We assign these decreases in percentages mainly to two causes: the effect of washing of particles, depending on their size, the solubility of the particles, and the metal compounds contained in them (*Mészáros*, 2002). About their size distribution, we know through our studies on the same samples, that the metals are more associated with the smallest size fraction (F particles) regarding the TSP concentrations, such as Ni (73%), V (70%), and Co (56%), although, other metals also have notable percentages, such as Mg (48%), Mn (44%), Ti (42%), and Fe (37%), always higher than in the percentages of coarse particles (*Fernández et al.*, 2001). These percentages would explain the large washing

effect on metals in the rainy day situations, including Fe and Ti, mainly on fine particles.

Table 3. Percentages of decreases of the concentrations of particles and metals by the rain regarding the dry days

	TSP	Ca	Fe	Mg	Pb	Cu	Mn	Ti	V	Ni	Co	Cd
A	-36.3	-51.8	-54.5	-9.8	-39.1	-29.8	-49.9	-50.4	-67.0	-44.7	+9.7	-22.9
B	-14.6	-47.3	-43.1	+16.4	-16.6	-17.7	-45.3	-42.0	-45.4	-49.2	-4.2	+14.2
C	+0.1	-3.7	-36.1	+26.3	-25.2	-2.9	-39.2	-39.5	-55.0	-22.2	+37.5	-10.7
D	-23.1	-2.4	-49.9	+5.4	-41.7	-1.7	-51.2	-50.6	-50.7	-39.0	+23.6	-20.9
E	-41.0	-2.2	-62.2	-17.4	-49.8	-11.1	-54.7	-61.1	-48.0	-44.7	+82.4	-38.3
F	-50.9	+6.5	-71.1	-20.2	-30.6	-45.7	-59.9	-62.2	-57.6	-57.4	+33.2	-48.4
Total	**-39.1**	**-19.7**	**-58.1**	**-7.8**	**-32.2**	**-27.0**	**-53.8**	**-54.1**	**-56.3**	**-53.8**	**+29.1**	**-39.3**

With regards to solubility, we know through our chemical speciation studies corresponding to these fine particles samples, that the metals with higher percentages in the soluble chemical forms regarding the total concentrations are those of V (50%), Ni (40%), Co (35%), and Mn (33%), but not those of Fe (4%), Ti (8%), and Mg (18%) (*Fernández et al.*, 2002). These percentages would explain the large decreases in the sample concentrations for the metals V, Ni, and Mn in rainy day situations, specially regarding the high soluble capacity of vanadium. The metals Fe and Ti are not particularly soluble, however, both are removed well enough by rain. Their percentages of decrease in the fine fraction are 71.1% and 62.2%, respectively, higher than V, Ni, and Mn (*Table 3*). Therefore, in the case of Fe and Ti, the removal effect that prevails is the physical washing, since their percentages of the fine fraction from the TSP is greater than the 37%, as mentioned above.

Thus, the removal mechanism most probably combines the physical effect of washing by the drops of rain that fall, together with the solvent effect of the drops of water, which dissolve the soluble compounds that form particles and metals. Additionally, the dissolved and washed metals and particles can also haul other chemical forms and particles with them.

With regard to cobalt metal, it is a highly soluble metal and accumulates in the fine particles, however, with higher concentration in the rainy samples. We found an explanation for this contrary behavior: There is a well-known special characteristic of the complexes of cobalt formed by cobalt (II) chloride and water molecules, they reflect pink colors with water and blue colors without water. If there is increasing rain, the concentration of water molecules

that surround the cobalt salts and complexes also increases, and the cobalt mixes with the humid air.

On the other hand, correlations of the rainy days matrix (*Table 2-c*) show only the total concentration of vanadium is clearly dependent on rain quantity ($r = -0.54$), and the higher anticorrelations of its size fractions (*Table 4-c*) correspond to particles larger than 4.9 μm, mainly the V2 fraction ($r = -0.60$) and V6 fraction ($r = -0.57$). Although, other size fractions are anticorrelated, as in the case of magnesium >4.9 μm ($r = -0.66$ for Mg1 fraction), Fe >10 μm ($r = -0.60$), Mn >4.9 μm ($r = -0.58$ for Mn1 and Mn2 fraction), and Ti >10 μm ($r = -0.57$), showing that the correlation is always with coarse sizes. Elimination of those sizes is dependent on the value of rainfall, with the exception of vanadium.

Both indicators of decreases in particle-metal levels by rain, percentages (*Fig. 2* and *Table 3*), and correlation coefficients (*Tables 2* and *4*) show that these fractionated particles and metals cited are those that have the same response in the rain. In general, it has been possible to observe that particles and metals of different sizes show different behavior in the rain. Differential responses from other parameters should be verified, as has been done for rain.

3.2.2 Influence of the remaining meteorological parameters on particle and metal concentrations and their size distributions

Firstly, the highest TSP values were observed proceeding from the most frequent wind direction, south and mainly southwest, but not from the strong western winds nor the low eastern winds, as can be seen in the Box & Whisker plot of *Fig. 1b*. Another six Box & Whisker plots, which are not represented here for all particle size fractions show, that F particles follow the same wind direction pattern as TSP with higher levels from the south. This trend is also sharper for A particles but mainly for B particles, both are coarse particles.

The effect, that the wind speed could reduce the TSP concentrations in the air by a removal effect from the airborne particles, is an anticorrelation, but it could also increase their levels if the wind resuspends coarse soil particles, showing positive correlation. This opposite effect should be the cause of the correlation coefficient between the two variables, both being low, although it is negative ($r = -0.39$) in the total matrix and rainy situations ($r = -0.36$), and null in dry situations ($r = +0.03$, *Table 2*). However, observing the size fraction data, in the rainy day situations only the fine particles between 1.3 and 0.6 μm present a clear negative coefficient (*Table 2-c*, $r = -0.66$). Therefore, these particles are those that were better dispersed by winds only in rainy situations. In *Table 2-a* the rain have a relationship with high wind speed

(r = + 0.54) and anticyclonic conditions, i.e., lower temperatures (r = - 0.51) and atmospheric pressures (r = - 0.66).

Regarding the total metal concentrations, *Table 2* shows in the total matrix that Cd was the most easily eliminated by the wind (r = - 0.56). Other metals have similar but lower anticorrelations, such as Ti (r = - 0.51), Ni (r = - 0.50), Mn (r = - 0.47), and Fe (r = - 0.46) in the same matrix, and Cd again (r = - 0.47) in dry samples. Cd is the only metal that appears with high anticorrelations in the three matrices.

Table 4. Results of the single linear regression (SLR) for the fractionated metals (FM) in function of the meteorological variables. Table contains the higher values of the coefficient r for each metal

Variable	Equation (Y = a + b X)	Correlation coefficient (r)	t_{calc}	Degrees of freedom	t_{tab}
	(a) Total matrix (41 samples)				
Mn4	Mn4 = - 0.63 + 0.08 AT	+0.69	5.95	39	2.02
Fe5	Fe5 = - 24.89 + 2.57 AT	+0.66	5.49	39	2.02
Ti5	Ti5 = - 0.23 + 0.03 AT	+0.66	5.49	39	2.02
Cd6	Cd6 = 0.39 - 0.02 WS	- 0.50	3.61	39	2.02
Ti5	Ti5 = 0.56 - 0.03 WS	- 0.66	5.49	39	2.02
Ni1	Ni1 = 0.31 - 0.02 WS	- 0.55	4.11	39	2.02
Mn5	Mn5 = 1.47 - 0.07 WS	- 0.54	4.01	39	2.02
Fe5	Fe5 = 50.18 - 2.66 WS	- 0.56	4.22	39	2.02
	(b) Dry days matrix (25 samples)				
Co3	Co3 = 0.18 - 0.01 AT	- 0.58	3.41	23	2.07
Mn1	Mn1 = 495.14 - 0.49 AP	- 0.70	4.70	23	2.07
Fe5	Fe5 = 3357.00 - 3.30 AP	- 0.60	3.60	23	2.07
Ti5	Ti5 = 29.57 - 0.03 AP	- 0.56	3.24	23	2.07
Ni6	Ni6 = 172.41 - 0.17 AP	- 0.54	3.08	23	2.07
V5	V5 = 86.93 - 0.09 AP	- 0.58	3.41	23	2.07
Cd5	Cd5 = 0.08 - 0.01 WS	- 0.50	2.77	23	2.07
Ni1	Ni1 = 0.37 - 0.03 WS	- 0.60	3.60	23	2.07
	(c) Rainy days matrix (16 samples)				
V2	V2 = 0.56 - 0.01 PP	- 0.60	2.81	14	2.15
V6	V6 = 3.69 - 0.11 PP	- 0.57	2.60	14	2.15
Mg1	Mg1 = 79.01 - 1.44 PP	- 0.66	3.29	14	2.15
Fe1	Fe1 = 120.23 - 3.02 PP	- 0.60	2.81	14	2.15
Mn1	Mn1 = 3.01 - 0.08 PP	- 0.58	2.66	14	2.15
Mn2	Mn2 = 2.57 - 0.05 PP	- 0.58	2.66	14	2.15
Ti1	Ti1 = 1.25 - 0.03 PP	- 0.57	2.60	14	2.15
Fe1	Fe1 = - 361.40 + 24.93 AT	+0.62	2.96	14	2.15
V1	V1 = - 1.55 + 0.10 AT	+0.64	3.12	14	2.15
Cd6	Cd6 = 0.29 - 0.01 WS	- 0.62	2.96	14	2.15
Ti2	Ti2 = 1.84 - 0.08 WS	- 0.57	2.60	14	2.15

About their size fractions, Cd was associated with the fine particles, <0.6 μm, in the total matrix ($r = -0.50$, *Table 4-a*) and in rainy situations ($r = -0.62$, *Table 4-c*), and with the fine particles between 1.3 and 0.6 μm in dry situations ($r = -0.50$, *Table 4-b*). This latter size, the E fraction was also associated with other metals, such as Ti, Mn, and Fe ($r = -0.66$, $r = -0.54$, and $r = -0.56$, *Table 4-a*). Ni was the only metal found in the coarse particles, >10 μm, ($r = -0.55$, *Table 4-a*; $r = -0.60$, *Table 4-b*). Finally, Ti presented high anticorrelations in rainy situations (*Table 4-c*) in the coarse particles, between 10 and 4.9 μm ($r = -0.57$). The majority of anticorrelations correspond to fine particles, <1.3 μm, mainly the E particles, except for the coarse particles, >4.9 μm, of Ni and Ti. Therefore, the particles most easily removed by the wind, as in the effect of rain, are the PM1 particles, fortunately.

On the other hand, significant positive correlations were found between temperature and TSP levels, i.e., the particle levels being high when temperatures were also high or vice versa. This correlation is well highlighted in the total matrix ($r = +0.62$), but also on the rainy days ($r = +0.50$) and slightly on the dry days ($r = +0.47$) (*Table 2*), therefore, this effect is marked and frequent. The mechanism is logical: when temperature is high, the density and viscosity of air diminish, and this favors the resuspension of particles. In the total matrix, particles smaller than 2.7 μm better correlated with the temperature, mainly the F particles ($r = +0.64$). In the dry samples, the particles <2.7 μm again better correlated with the temperature ($r = +0.53$ for D particles), and in the rainy situations only particles <0.6 μm ($r = +0.59$), correlated the best with the temperature. Therefore, the effect of temperature is more accentuated in the particles of less than 2.7 μm, although this would not be applied to extremely fine particles (e.g., $D_p < 0.1$ μm), because at this size there is not any resuspension.

The resuspension of particles by high temperatures could be attributed to a drying effect on earth crustal particles of soils and additionally to a decrease in air density and viscosity. Both reasons could facilitate the suspension of particles in the air. Our Regional Government is also aware of these episodes, since the particle concentration often exceeds the level of "not acceptable air quality" in its Air Control and Monitoring Stations. The other coherent explanation could be the Saharan particles coming from the North African warm winds. Also, at high temperatures an important production of fine particles occurs. Therefore, all three suppositions can be valid, and the third is in agreement with the experience of our regional episodes. The first two explanations are in agreement with the present particle size study, because it is most likely that the Saharan particles are coarse when they reach the continent (*Schütz* and *Sebert*, 1987; *Molinaroli et al.*, 1993). This problem exists not only in our city but also in other cities of our region of Andalusia. The

Saharan input represents a problem in other Mediterranean countries, including as far away as Central Europe. Therefore, the new Directive contemplates the possibility of keeping in focus the different geographical situations (Article 5.4 of the *Council Directive 1999/30/EC*, 1999).

Studying the relationship between temperatures and metal concentrations, one found that earth crustal metals such as Mn, Fe, and Ti had high concentrations at high temperature values ($r = +0.64$, $r = +0.61$, $r = +0.59$, respectively, *Table 2-a*). This fact supports the two explanations above mentioned, because both particle sizes are coming from earth crustal sources. When we studied their size distribution (*Table 4-a*), we observed that the effect rebounded on Fe5 particles ($r = +0.66$), Mn4 particles ($r = +0.69$), and particles of Ti <2.7 μm, mainly Ti5 ($r = +0.66$), i.e., the fine metal fractions again, contained in PM2.5. However, in rainy samples (*Table 4-c*), the size fractions, that have high correlation, are the particles >10 μm, such as Fe1 ($r = +0.62$) and V1 ($r = +0.64$), i.e., the coarse particles that respond to high temperatures in rainy situations.

On the other hand, we observed (*Table 2-b*), that, contrarily, cobalt was negatively correlated with temperature ($r = -0.65$), showing behavior opposite to that of TSP, Mn, Fe, and Ti. The size fraction that followed this trend was represented by particles between 4.9–2.7 μm ($r = -0.58$, *Table 4-b*). The explanation could be related to the stability of the cobalt complexes in the rainy situations mentioned above. Since temperature is negatively correlated with rainfall and cobalt is positively correlated with rainfall, logically cobalt is anticorrelated with temperature.

Regarding the atmospheric pressure parameter, the correlation study also reveal a dispersion effect on TSP (*Table 2-b*, $r = -0.67$). This effect of he anticyclonic conditions was strongest for the fine E particles (*Table 2-b*, $r = -0.67$), but the anticorrelations are high for all size fractions.

There were also several anticorrelations for metal concentrations (*Table 2-b*), with Mn ($r = -0.69$), Fe ($r = -0.61$), Ti ($r = -0.57$), Ni ($r = -0.57$), and V ($r = -0.55$). Studying their size distribution (*Table 4-b*) we found, that predominant size fractions for Mn were particles >4.9 μm ($r = -0.70$ for Mn1 particles), particles < 1.3 μm for Fe ($r = -0.60$ for Fe5 particles), Ti5 particles ($r = -0.56$), Ni6 particles ($r = -0.54$), and V5 and V6 particles ($r = -0.58$ for V5 particles).

One can observe that the metals having correlations or anticorrelations with the main meteorological parameters are always the earth crustal elements Fe, Ti, and Mn. In these cases not only fine particles were highly correlated, but also the coarse particles in several metals.

Correlations and anticorrelations of particles metals, and their size fractions were found, which could explain several relationships with

meteorological parameters. Atmospheric pressure has shown stronger dispersion effect than wind speeds on suspended particles and metals, and temperature shows a contrary effect on concentration. But, in some analytical variables there are negative and positive correlations at the same time. For example, in the rainy matrix, vanadium is correlated with ambient temperature and anticorrelated with atmospheric pressure, and the same fact occurs in total and dry matrices with TSP, Fe, Mn, Ti, and Ni concentrations. Therefore, what will the global behavior of these elements be, faced with both parameters at the same time? This question can not be answered by single correlations, but with multiple regressions.

3.3 Multiple linear regression analysis to correlate the behavior of variables with meteorological conditions

In the previous section, we found significant correlations between analytical variables and meteorological data through simple linear regression (SLR) analyses, mainly with rainfall, temperature, and atmospheric pressure. As expected, it was also possible to find multivariate equations to relate only the correlated variables in the SLR (*Tables 2* and *4*) with all the meteorological parameters at the same time using the multiple linear regression (MLR) analysis (*Fernández et al.*, 2000). These equations can be useful in verification if the concentrations in the air can follow a basic model of behavior for particles metals, and their size fractions, and if this model is more accurate than the SLR. Therefore, applying the *Statistica* package we obtained these equations for the three matrices (*Table 5*). This table shows, also underlined, the significant coefficients for meteorological parameters.

One can observe in *Table 5*, that the equations that give the worst correlation coefficients for TSP concentrations are those obtained for the rainy days matrix ($r = 0.60$). Consequently, the coefficient is lower for the total matrix ($r = 0.71$), which contains rainy samples, than for the dry days matrix ($r = 0.74$), without rainy samples. This is also evidence, that rain situations distort the study of atmospheric pollution a lot by total suspended particles. This difference can be verified in *Fig. 3-b,c*, where the poor capacity of prediction of the equation on rainy days can be seen in relation to the dry days. This fact should be due to the different behaviors of the different size fractions in rainy situations most influenced by the rain. Thus, variability (*Table 1*) in rainfall variable (168 %) is greater than wind speed (44%) for example, and, therefore, the success of prediction is lower. Only several fractions of soluble elements such as magnesium or vanadium (*Fig. 3-f*) have a better capacity for prediction in rainy day matrices.

Table 5. Results of the multiple linear regression (MLR) for the TSP, FSP, TM, and FM variables in function of all meteorological variables. The table underlines the significant coefficients for meteorological parameters

Variable (Y)*	a	b_1	b_2	b_3	b_4	Correlation coefficient (r)	t_{calc}	Degrees of freedom	t_{tab}
(a) Total matrix (41 samples)									
TSP	3469.328	-1.787	-0.672	4.091	-3.426	0.7128	6.35	36	2.028
F	1334.967	-1.015	0.208	3.036	-1.339	0.6855	5.88	36	2.028
Mn	497.983	-0.427	-0.264	0.914	-0.491	0.7212	6.50	36	2.028
Mn4	1.569	-0.013	-0.020	0.056	-0.001	0.7372	6.81	36	2.028
Fe	22467.817	-19.666	-13.169	35.747	-22.125	0.7001	6.12	36	2.028
Fe5	469.961	-0.509	-1.124	1.720	-0.461	0.7323	6.72	36	2.028
Ti	166.131	-0.154	-0.230	0.311	-0.161	0.6766	5.74	36	2.028
Ti5	3.216	-0.004	-0.018	0.015	-0.003	0.7655	7.43	36	2.028
Cd	8.653	0.001	-0.027	0.016	-0.008	0.6323	5.10	36	2.028
Cd6	4.314	0.000	-0.016	0.014	-0.004	0.5874	4.53	36	2.028
Ni	90.505	-0.055	-0.096	0.069	-0.088	0.6448	5.27	36	2.028
Ni1	8.579	-0.001	-0.022	0.001	-0.008	0.5891	4.55	36	2.028
(b) Dry days matrix (25 samples)									
TSP	7485.992	-	1.414	2.663	-7.367	0.7421	6.91	21	2.080
E	363.016	-	0.091	0.145	-0.358	0.7606	7.32	21	2.080
Co	13.169	-	-0.006	-0.038	-0.012	0.6682	5.61	21	2.080
Co3	-1.808	-	0.000	-0.006	0.002	0.5902	4.57	21	2.080
Mn	1830.889	-	-0.017	0.525	-1.799	0.7448	6.97	21	2.080
Mn1	468.513	-	-0.199	0.046	-0.459	0.7741	7.64	21	2.080
Fe	74643.533	-	6.169	17.149	-73.283	0.6445	5.26	21	2.080
Fe6	34607.535	-	16.263	10.551	-34.147	0.6710	5.65	21	2.080
Ti	681.318	-	-0.020	0.137	-0.667	0.5946	4.62	21	2.080
Ti5	25.812	-	-0.012	0.007	-0.025	0.6597	5.48	21	2.080
Ni	242.965	-	-0.059	0.017	-0.237	0.5917	4.58	21	2.080
Ni1	23.130	-	-0.031	-0.004	-0.022	0.7211	6.50	21	2.080
V	1064.356	-	-0.220	-0.145	-1.039	0.5769	4.41	21	2.080
V1	103.101	-	-0.064	-0.019	-0.100	0.6781	5.76	21	2.080
Cd	16.048	-	-0.032	0.014	-0.016	0.5874	4.53	21	2.080
Cd5	1.352	-	-0.006	0.002	-0.001	0.5707	4.34	21	2.080
(c) Rainy days matrix (16 samples)									
TSP	255.600	-0.453	-3.053	7.313	-0.287	0.5996	4.68	11	2.201
B	715.802	-0.182	-0.108	0.285	-0.701	0.7330	6.73	11	2.201
V	-416.026	-0.074	-0.410	0.943	0.406	0.7308	6.69	11	2.201
V2	-2.096	-0.010	-0.048	0.058	0.002	0.8293	9.27	11	2.201
Mg1	6487.662	-1.840	5.547	-1.105	-6.403	0.8180	8.88	11	2.201
Fe	-16502.994	-3.521	-24.701	78.671	15.682	0.6804	5.80	11	2.201
Fe1	-2304.284	-1.997	-5.962	16.904	2.163	0.7630	7.37	11	2.201
Mn1	-214.868	-0.071	-0.134	-0.006	0.218	0.6949	6.03	11	2.201
Ti1	-56.542	-0.019	-0.107	0.064	0.057	0.7333	6.74	11	2.201
Cd6	-3.824	0.000	-0.017	0.000	0.004	0.6364	5.15	11	2.201

*: Equation: $Y = a + b_1 PP + b_2 WS + b_3 AT + b_4 AP$

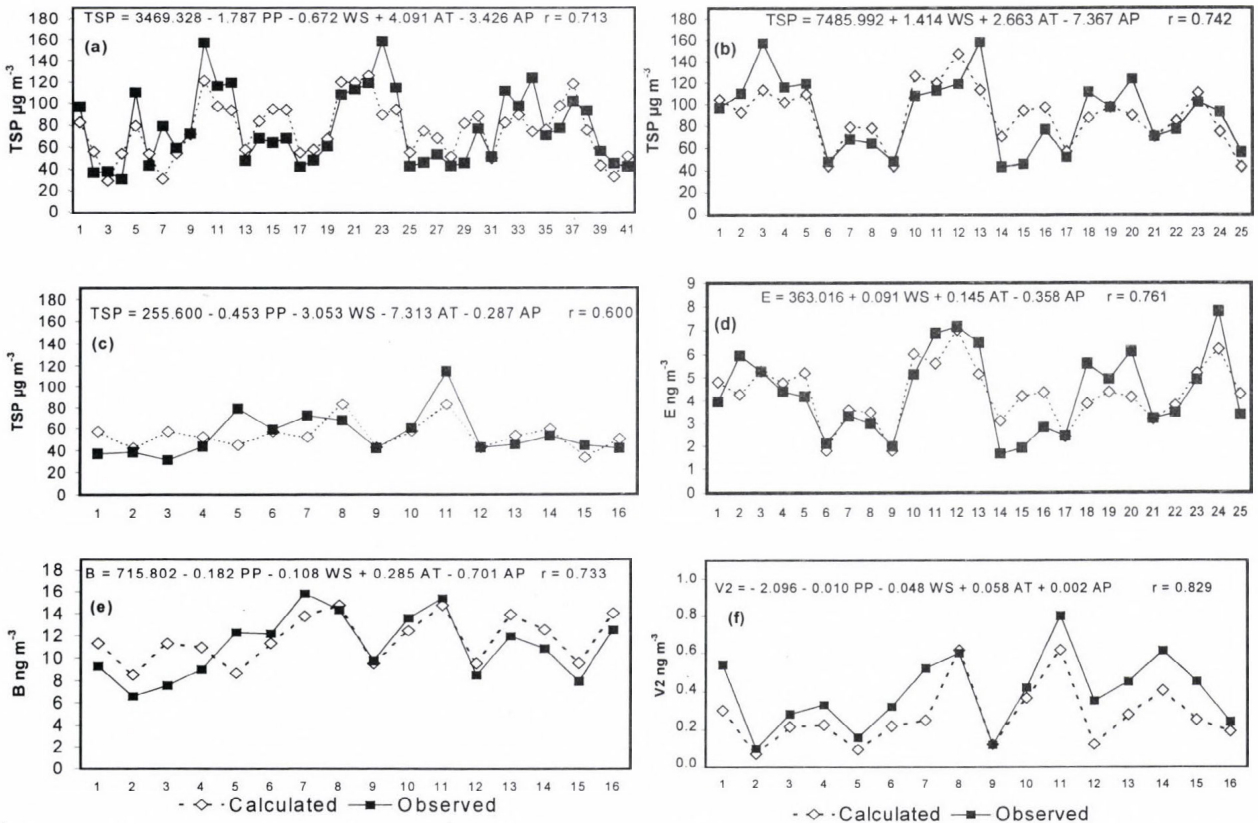

Fig. 3. Comparison between concentrations of the experimental values of analytical parameters and the corresponding predicted values for (*a*) TSP in total matrix, (*b*) TSP in dry days matrix, (*c*) TSP in rainy days matrix, (*d*) E particles in dry days matrix, (*e*) B particles in rainy days matrix, and (*f*) V2 in rainy days matrix.

Regarding the size fractions of particles, in the dry days matrix, the E particles are most highly correlated (r = 0.76). These particles are those, in which more correlation and anticorrelation were found, therefore, they are the particle sizes most influenced by meteorological parameters. In both, total and dry matrices, the fine particles (E and F fractions) are the most easily predicted (*Fig. 3-d* for the E particles). However, in rainy situations, the coarse particles are the best correlated, the A and B particles instead of fine particles (*Fig. 3-e* for B particles). This fact is in accordance with the fact that the coarse particles are those that respond positively to the amount of rainfall, although the fine particles are those that are best removed by the rain independently of the rainfall. Thus, the rainy situations introduce a major difficulty when predicting the behavior or concentrations of fine particles, which are the most harmful.

Regarding the total metal and their size fraction concentrations, in dry and total matrices the metal with the highest correlation is manganese (r = + 0.74 and r = + 0.72, *Table 5*), but on rainy days vanadium (r = + 0.73) is the metal that was found to be a model of behavior more accurate than the SLR. Meanwhile, manganese does not appear in the rainy days matrix because of its low coefficient (r is significantly equal to zero). The metal iron is the only one that appears with a coefficient higher than 0.64 in the three matrices, and is also the only one that has a higher correlation coefficient in the rainy days matrix (r = + 0.68), although with smaller differences, than in the dry days matrix (r = + 0.64).

The corresponding size fractions of metals have generally higher coefficients than the total concentrations, except for several cases, such as Cd6 and Ni1 in the total matrix, and Co3 or Cd5 in the dry days matrix. Many of these coefficients are high or extremely high, for example, Ti5, Mn4, and Fe5 in the total matrix, Mn1 and Ni1 in the dry days matrix, and Fe1, Ti1, and mainly V2 and Mg1 in rainy days matrix, with coefficients higher than 0.82. These metal fractions are the best explained in both matrices (*Table 5*).

These results confirm again the importance of the relationship of the meteorological parameters with the particles and metals depending on their corresponding sizes.

4. Conclusions

Interesting interrelations were found that explain the behavior of particles and metals of different sizes in different meteorological conditions: the effect of temperature on the increase of particle concentrations, the effect of

atmospheric pressure and wind speed on the dispersion of particles, and the elimination of particles by the rain.

Multiple linear regression technique was notably useful to confirm the poor capacity of prediction on rainy day conditions for particles and metals. The best prediction was observed for metals that can be in soluble forms in the air, such as magnesium and vanadium. The particles lower than 1.3 micrometers are the most easily predicted when studying the size distribution of particles. The metal concentrations with the highest correlation coefficients in the MLR were observed for fine particles, such as the Fe, Mn, and Ti metals, or coarse particles, such as the Mn, Ni, Mg, Fe, V, and Ti metals.

We conclude that rainfall is the meteorological parameter that most affects particle elimination and metal pollution by physical and chemical washing away of particles. The other meteorological parameters were also observed influencing the presence of different size particles in the air (wind speed, temperature, and pressure). These effects are different for different size fractions.

It would be interesting to extrapolate from these methods, if used in other regions and countries, to the possible data, checking the differences and similarities with their results. Although, our first objective after this study will be to repeat this research for a longer time period with a larger number of samples and several additional meteorological parameters. The study of the size distribution and meteorological parameters constitutes a way to increase the information about the lifetimes of pollutants in the urban air. The satisfactory results of the multiple linear regression technique should be checked into a context of a wide research with a wide sampling period.

Acknowledgements—We would like to thank the "Consejería de Medio Ambiente de la Junta de Andalucía" for their financial assistance in carrying out this research project.

References

Brooks, L. and *Salop, J.*, 1983: Chemical and meteorological characteristics of atmospheric particulates in southeastern Virginia utilizing multi-variant analysis. *J. Air Control Association 33*, 222-224.

Choularton, T W., Fullarton, G., and *Gay, M.J.*, 1982: Some observations of the influence of meteorological variables on the size distribution of natural aerosol particles. *Atmospheric Environment 16*, 315-323.

Council Directive 1999/30/EC of 22 April, 1999: Relating to limit values for sulphur dioxide, nitrogen dioxide and oxides of nitrogen, particulate matter and lead in ambient air. Official Journal L163, 41-60.

Despiau, S., Cougnenc, S., and *Resch, F.*, 1996: Concentrations and size distributions of aerosol particles in coastal zone. *J. Aerosol Science 27*, 403-415.

Elsom, D.M. and *Chandler, T.J.*, 1978: Meteorological controls on ground level concentrations of smoke and sulphur dioxide in two urban areas of the U.K. *Atmos. Environ. 12*, 1543-1554.

Fernández, A.J., Ternero, M., Barragán, F.J., and *Jiménez, J.C.*, 1999: Source characterization of airborne particles in Seville (Spain) by multivariate statistical analyses. *Időjárás 103*, 261-273.

Fernández, A.J., Ternero, M., Barragán, F.J. and *Jiménez, J.C.*, 2000: An approach to characterization of urban airborne particles sources through heavy metals speciation. *Chemosphere 2*, 123-136.

Fernández, A.J., Ternero, M., Barragán, F.J., and *Jiménez, J.C.*, 2001: Size distribution of metals in urban aerosols in Seville (Spain). *Atmospheric Environment 35*, 2595-2601.

Fernández, A.J., Ternero, M., Barragán, F.J., and *Jiménez, J.C.*, 2002: A chemical speciation of trace metals for fine urban particles. *Atmospheric Environment 36*, 773-780.

ISO 7708, 1995: *Air Quality - Particle Size Fraction Definitions for Health-related Sampling*. ISO Publications, First Edition 1995-04-01.

Melgarejo, P.L., Ternero, M., and *Gracia, I.*, 1986: A study of the atmospheric lead pollution in Sevilla, Spain. Influence of meteorology and traffic, and relationship with other traffic-generated pollutants. *Int. J. Env. Analytical Chemistry 24*, 283-296.

Mészáros, E., 2002: Atmospheric wet deposition as a nutrient supply for the vegetation. *Időjárás 106*, 103-111.

MMA, Ministerio de Medio Ambiente, 1997: *Guía resumida del clima en Espa a 1961-1990.* Dirección General del Instituto Nacional de Meteorología. Edita Secretaría Técnica de Medio Ambiente, Madrid.

Molinaroli, E., Guerzoni, S., and *Rampazzo, G.*, 1993: Contribution of Saharan dust to the Central Mediterranean basin. In *Proc. Controlling the Composition of Clastic Sediments* (eds.: *M.J. Johnsson* and *A. Basu*). *Geological Society of America. Bulletin* Special Paper, 303312.

Schütz, L. and *Sebert, M.*, 1987: Mineral aerosols and source identification. *J. Aerosol Science 18*, 1-10.

StatSoft, Inc., 1999: *STATISTICA' 99* Edition for Windows (Computer program), Kernel release 5.5. Tulsa, OK, USA.

Usero, J., Rosa, F., Ternero, M., and *Gracia, I.*, 1988: A determination of the sources in the Seville urban aerosol. *Int. J. Env. Analytical Chemistry 33*, 233-244.

Väkevä, M., Hämeri, K., Puhakka, T., Nilsson, E.D., Hohti, H., and *Mäkelä, J.M.*, 2000: Effects of meteorological processes on aerosol particle size distribution in an urban background area. *J. Geophysycal Research 105(D8)*, 9807-9821.

Witz, S. and *Moore, A.B.*, 1981: Effect of meteorology on the atmospheric concentrations of traffic-related pollutants at a Los Angeles Site. *J. Air Pollution Control Association 31*, 1098-1101.

IDŐJÁRÁS

Quarterly Journal of the Hungarian Meteorological Service
Vol. 108, No. 1, January–March 2004, pp. 33–49

Nowcasting of the precipitation type Part II: Forecast of thunderstorms and hailstone size

István Geresdi[1], **Ákos Horváth**[2] and **Árpád Mátyus**[1]

[1]*University of Pécs, Institute of Geography,*
Ifjúság u. 6, H-7624 Pécs, Hungary; E-mail: geresdi@ttk.pte.hu

[2]*Hungarian Meteorological Service,*
Vitorlás u. 17, H-8600 Siófok, Hungary; E-mail: horvath.a@met.hu

(Manuscript received May 23, 2003; in final form December 22, 2003)

Abstract—The purpose of this research was to develop a numerical model to estimate the occurrence of thunderstorms and hailstones on the ground. This model is a part of the nowcasting system (MEANDER) developed by the Hungarian Meteorological Service. The formation of the thunderstorms was estimated by running a one-dimensional, steady state model at every grid point of the mesh covering the Carpathian Basin. Using sounding and surface data over a grid with 3 km horizontal resolution initialized the model. The outputs of the model are: vertical profile of temperature and updraft velocity of the ascending air parcel, furthermore, the size of the largest hailstone on the ground. Convective Available Potential Energy (CAPE) is also calculated to estimate convective activity. The predicted occurrence of the thunderstorms was compared to radar observations. The calculated maximum hailstone sizes were checked by using reports of the voluntary observers. The comparisons show that nowcasting system overestimates the occurrence of the thunderstorm formation; about 20% of the alarms were false. In most cases the nowcasting system forecasted the formation of the thunderstorms one hour before they appeared.

Key-words: nowcasting, numerical simulation, thunderstorm, hailstone, radar observation.

1. Introduction

In the second part of this series the results about the convective activity are published. In the first part (*Geresdi* and *Horváth*, 2000) we dealt with the winter precipitation. Now, we are focusing on the characteristic phenomenon of the summer weather, the thunderstorm. Strong convective storms frequently

produce large hail and intensive outflow. Both phenomena are consequence of very complicated and strongly interacting dynamics and microphysical processes. Two possible approximations could be used to simulate the development of convective storms. It is obvious that the mesoscale models with high horizontal resolution (distance between grid points in the horizontal direction should be about 1 km) and sophisticated microphysical description could be the most appropriate for modeling of this process (e.g., *Pilke et al.*, 1992; *Colle* and *Clifford*, 2000). Although the mesoscale models have number of advantages, because of the necessary high horizontal resolution, it takes order of hours to give a three-hour forecast. Another possibility is the application of a highly parameterized scheme to simulate the dynamics (e.g., *Aleksic et al.*, 1991), and using the available computer capacity to give a more detailed microphysical description about the process we focus on. In this project we chose the second way. The dynamics of the convective clouds is characterized by the output of a one-dimensional steady state cloud model with bulk microphysics. A detailed microphysics is used to calculate the melting rate of the falling hailstone.

The output data of the model occurrence of thunderstorms and maximum hailstone size - was compared with radar observation, and surface reports of hailstones. The output of the thunderstorm nowcasting is described by presentation of a case study.

2. Description of the model

One-dimensional steady state cloud model is used to characterize the updraft region of convective clouds. The updraft velocity (w) of the ascending air parcel is determined by the buoyancy, lateral entrainment and weight of the hydrometeors:

$$\frac{dw}{dz} = \frac{g}{w}\left(\frac{T_{vc} - T_{ve}}{T_{ve}} \frac{1}{1+\alpha} - q\right) - \mu w, \tag{1}$$

where q is the mixing ratio of hydrometeors, T_{vc} and T_{ve} are the virtual temperature inside and outside of the air parcel, respectively. α is a correction parameter (0.5), which compensates the neglect of nonhydrostatic pressure perturbations (*Anthens*, 1977). The entrainment rate (μ) is directly proportional to the updraft velocity (w) and inversely proportional to the radius of the air parcel. The entraining air with cooler temperature and lower vapor content effects the total water content and temperature of the air parcel as well. Beside the water vapor, five types of water substances are considered: cloud water, cloud ice, snow, rain, and hail/graupel. Interactions between these substances

are simulated by bulk microphysics. The fall out of the precipitation particles is not allowed. The heat released during the freezing of supercooled drops, condensation, and deposition increases the temperature of the ascending air parcel. For estimation of the convective activity, the CAPE was calculated by taking into consideration that the temperature of the air parcel in addition to the releasing latent heat of condensation is affected by the entrainment of the cooler and dryer environmental air and by the releasing latent heat of fusion. More details about the model could be found in *Zoltán* and *Geresdi* (1984).

The one-dimensional steady state simulation describes the dynamics of the updraft core. Modifying the initial parameters of the ascending air parcel (e.g., temperature, radius, updraft velocity), it could be achieved that the calculated cloud top height agrees well with the radar observation (*Marwitz*, 1970). While the height of the cloud top is well observable parameter, unfortunately only a few measurements are available for the vertical updraft profile in convective storms. The reason of the absence of this type of data is that synchronization of two or three Doppler radars is necessary for measurement of the three-dimensional velocity field. The basic theory of the application of one-dimensional models for estimation of convective activity is that the good agreement between the observed and calculated maximum cloud top height means that the model calculates well the maximum updraft velocity as well (*Foot* and *Mohr*, 1979). The updraft velocity has a strong effect on the precipitation formation in convective clouds. The fast lifting of the air may results in low precipitation formation efficiency of the convective clouds (*Fankhauser*, 1988).

Although the hailstones spend most of their life time outside of the most intensive area of the updraft core, their size seems to be well correlated with the maximum of updraft velocity. However, the size of the hailstone on the ground is not only effected by the intensity of the storm, but the mass of the hail could be significantly reduced due to the melting between the 0°C level and the ground. A numerical model, which involves both of the above mentioned effects, was developed to estimate the maximum size of hailstones on the ground. The equation for initial radius of the largest hail particle comes from the assumption that the terminal velocity of the largest hailstones – could form in the cloud – is equal to the maximum of the updraft velocity:

$$w_{\max} = \sqrt{\frac{2\rho_h g d_{\max}}{3\rho_a c_d}}, \tag{2}$$

where $w_{\max}$ is the calculated maximum updraft velocity. The right side of this equation is the terminal velocity of the hailstone with diameter of $d_{\max}$.

The density of the hailstone (ρ_h) generally changed between 450 kg/m^3 and 950 kg/m^3. Low density particles form when the hailstone formation is initiated by aggregation of ice crystals, and the structure of the hailstone becomes porous. The density can increase over that of bulk ice if the melted water fills the pores. If hailstone forms from supercooled water drops with size of few millimeters and grows by collection of supercooled drops, its density is near to that of bulk ice. For simplicity, density of 900 kg/m^3 was used during the simulation. ρ_a is the density of air and c_d is drag coefficient (0.6).

Previous laboratory results show that the meltwater sheds from the ice core if the diameter of the hailstone is greater than 9 mm, and only a thin liquid layer remains on the surface of the hailstone (*Rasmussen et al.*, 1984). It is supposed that the falling particle does not collect either liquid or solid hydrometeors. Sensitivity studies made by *Rasmussen* and *Heymsfield* (1987b) shows that while collection of the liquid water hardly affects the melting rate, the low relative humidity significantly reduces it. If the heat transfer from the collected particles could be neglected, the melting rate depends only on the heat transfer from the ambient air and the heat released due to the diffusion of water vapor from the surface of the particle (*Rasmussen* and *Heymsfield*, 1987a):

$$\frac{dm_h}{dt} = \frac{1}{L_f}\{-4\pi r_h k_a (T_\infty - T_s) f_h - 4\pi r_h L D_v (\rho_{v,\infty} - \rho_{v,s}) f_v\}, \qquad (3)$$

where r_h is the radius of the hailstone, k_a and D_v are heat conductivity of air and vapor diffusion coefficients in air, respectively. T_∞ and T_s are the temperatures in the environment and on the surface of the graupel, $\rho_{v,\infty}$ and $\rho_{v,s}$ are the vapor densities far from the graupel and on its surface, respectively. The surface temperature of the melting hailstone is 273.15 K, and the vapor density at the surface is given by the saturation vapor pressure at the melting point. L_v and L_f are the latent heat of condensation and that of fusion, respectively. f_v and f_h are ventilation coefficients for vapor and heat transfer (*Pruppacher* and *Klett*, 1997), respectively:

$$f_v = 0.78 + 0.308 N_{Sc}^{1/3} N_{\mathrm{Re}}^{1/2},$$

$$f_h = 0.78 + 0.308 N_{Pr}^{1/3} N_{\mathrm{Re}}^{1/2},$$

where N_{Sc} and N_{Pr} are the Schmidt and Prandtl numbers. The first term between the brackets in Eq. (3) is the heat transfer due to the conduction; the

second term is the releasing latent heat due to vapor diffusion. The hailstone with initial size of d_{max} (Eq. (2)) starts to fall down from the height of the melting level. The time period, the melting particle spends between the melting level and the ground, depends on the terminal velocity of the falling particle and the strength of the downdraft. The terminal velocity is a function of the Reynolds number and was calculated on the base of the paper of *Rasmussen* and *Heymsfield* (1987a). Unfortunately, generally we have no data about velocity, vapor, and water content in the descending air. In the downdraft, due to the fall out effect and the strong mixing with environmental air, the water content could be significantly smaller than the adiabatic value. Because of this uncertainties the collision between the melting hailstones and water drops was not taken into consideration. Although the sensitivity studies show that the vapor content is an important parameter, unfortunately we have no information about how it changes in space and time. It is supposed that due to the evaporation of the raindrops the vapor content in the downdraft is near to the saturation value. This may not be true at the time, when the precipitation elements start to fall out from the cloud, but later the relative humidity should be near 100%. The ambient temperature of the falling hailstone was given by wet adiabatic descend starting from the level of -10°C, and the velocity of the descending air was supposed to be 5 m/s. In the downdraft of intensive storms this value could be higher, but it is generally less than 10 m/s. Underestimation of the downdraft overestimates the time period necessary for the hailstone to reach the ground, that is the melting of the hailstone is overestimated.

Fig. 1 shows the possible effects of these uncertainties on the calculated hailstone size. The effect of the downdraft intensity and that of the subsaturation were investigated by using three different downward velocities (0, 5, and 10 m/s) and three different values of relative humidity (80, 90, and 100%). The hailstone started to fall at height of 3.5 km with initial radius of 10 mm. That means that maximum updraft velocity in the convective storm where the hailstone formed was about 18 m/s. Due to the adiabatic warming the temperature of the air inside the downdraft increased from 0°C to 27°C. The hailstone lost only a few percent of its mass above the level of 2 km in every case. The explanation of the acceleration of the melting near to the ground is the larger air temperature and the increase of surface/mass ratio due to the melting. The shorter falling time period due to the increased downdraft velocity resulted in about 20% larger final hail size on the ground. The consequence of the lower of vapor content was also larger hail size. The larger the cooling rate caused by the evaporation from the surface of the hailstones, the larger the size of the hailstone was on the ground. Calculation was made also by relative humidity of 50%. In this case the size of the hail particle

hardly decreased and it was about 8.3 mm on the ground. However, low relative humidity like this is rarely observed in precipitation shaft.

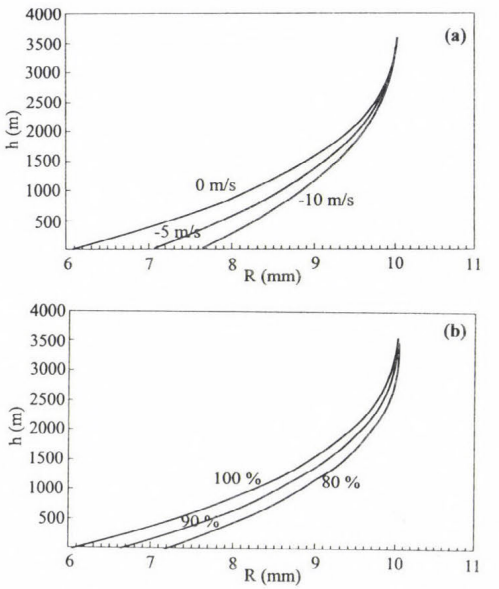

Fig. 1. Effect of downdraft (*a*) and relative humidity (*b*) on the melting of the hailstones. The calculation was made at three velocities of 0, 5, and 10 m/s, and with relative humidity of 100, 90, and 80%. The curves are denoted by the appropriate numbers. The downdraft was 0 m/s in all of the three cases in Fig. 1b.

3. Initialization

Input data of the model are produced by nowcasting system developed at the Hungarian Meteorological Service. The system uses real time data of surface observations (SYNOP), forecasted fields of a limited area model ALADIN (*Horányi et al.,* 1996), and calculates the objective analysis using optimal interpolation for data assimilation. Radar reflectivity data are also applied for analysis of relative humidity. The MEANDER (Mesoscale Analysis Nowcasting and Decision Routines) system produces high resolution (dx = dy = 3 km and dz = 200 m) 3D fields of basic parameters: pressure, geopotential height, temperature, relative humidity, and wind. We refer the reader to *Horváth* and *Geresdi* (2003) for more information about MEANDER.

The height and temperature of the condensation level are calculated by using dry adiabatic ascend from the ground. It is supposed that the air layer

above the ground is well mixed. The potential temperature and vapor content of the ascending air parcel are given by the following equations:

$$\bar{q}_{v,0} = \frac{1}{200}\int_0^{200} q_v(z)dz, \qquad \bar{\Theta}_0 = \frac{1}{200}\int_0^{200}\Theta(z)dz, \tag{4}$$

where the values of the $q_v(z)$ and $\Theta(z)$ functions are given by interpolation technique applied in MEANDER to calculate the parameters near the surface. The air parcel is initiated from the condensation level with radius of 5 km and updraft velocity of 5 m/s.

4. Application

Model output was compared with observations between May 1 and September 30, 2002, in southern part of Transdanubia (area of this region is about 840,000 ha). In this region of Hungary (target area) hail suppression has been carried out since early 90's. (Hungary is in central region of Europe bounded by longitudes of 16°19' and 22°48' and latitudes of 45°48' and 48°36'.) More details about the applied technique for the hail suppression could be read in *Dessens* (1986). S-band radar has been used to detect thunderstorms over the region. It was supposed that a thunderstorm formed if the maximum reflectivity of a cell reached 45 dBZ. Radar observations are compared with the calculated occurrence of thunderstorms. Reports of hail from the locations of the ground based generators are used to check the forecasted maximum hailstone size. (The mean distance between the generators is less than 10 km.) The nowcasting output is presented by a case study. On the August 4, 2002, an intensive precipitation system crossed the western part of the Hungary in southwest-northeast direction. This squall line was forecasted neither of the mesoscale models applied at the Hungarian Meteorological Service.

4.1 Case study of August 4

The synoptic analysis of the following case study is based on mean sea level pressure (mslp) and upper level (850 and 500 hPa) data of ECMWF analysis. In the morning of August 4, 2002, a cold front passed the Alpine region. At 06 UTC a prefrontal squall line appeared in the western part of Hungary (*Fig. 2a*). This squall line was indicated by line organized thunderstorms and moved from southwest to northeast. On the 850 hPa level, temperature and wind fields do not show significant cold or warm advection at 6 UTC (*Fig. 2b*), but on the 500 hPa level, massive cold advection can be recognized (*Fig. 2c*). At 12 UTC on the mslp chart, the squall line can be clearly divided from the cold

front (*Fig. 2d*). The cooling of the low level troposphere, caused by thunderstorms of the squall line, decreased the temperature gradient of cold front, that was the reason why only weak cold advection occurred on the 850 hPa level at 12 UTC above the investigated area (*Fig. 2e*). On the 500 hPa level, a characteristic cold trough could be recognized above the Carpathian Basin which was isolated from the western cold air mass (*Fig. 2f*). Definitely this high level, fast moving cold trough was responsible for increasing of convective components (*Horváth* and *Geresdi*, 2000), and after all for the formation of heavy thunderstorms. The height of the 0°C level was at about 3400 m (AGL) during the day.

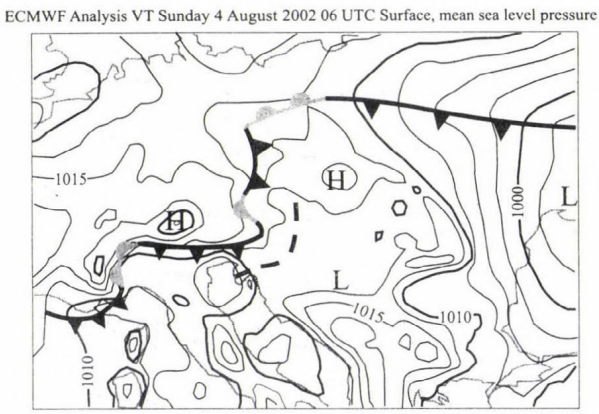

Fig. 2a. Mean sea level pressure field and front analysis at 06:00 UTC, August 4, 2002
The prefrontal squall line is close to the cold front.

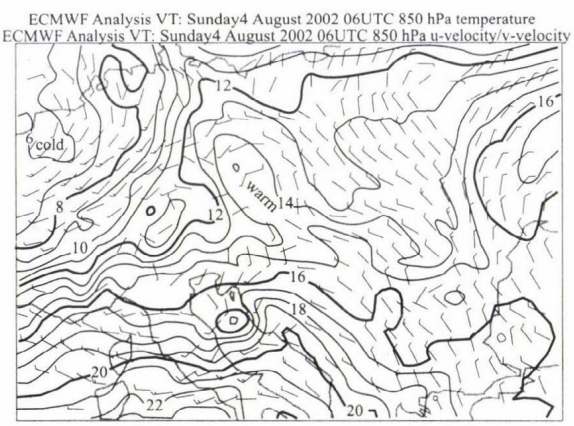

Fig. 2b. 850 hPa temperature and wind fields at 06:00 UTC, August 4, 2002.
There is no significant temperature advection.

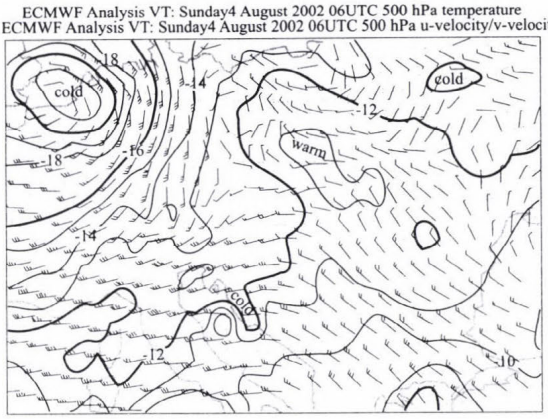

Fig. 2c. 500 hPa temperature and wind fields at 06:00 UTC, August 4, 2002. Characteristic cold advection can be recognized above the Carpathian Basin.

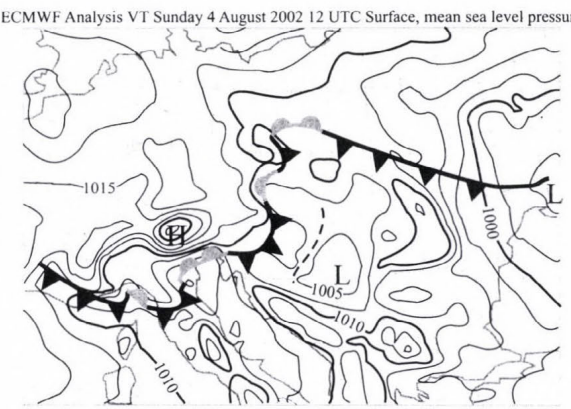

Fig. 2d. Mean sea level pressure field and front analysis at 12:00 UTC, August 4, 2002. The prefrontal squall line is well separated from the cold front.

The typical output of the nowcasting system are shown in *Fig. 3* and *Fig. 4*. The convective activity is characterized by the CAPE (*Fig. 3*), which was calculated by the one-dimensional, steady state numerical model. This figure shows the isolines for the CAPE at the time when the convective activity reached its daily maximum. Due to the large instability, formation of severe thunderstorms could be expected in an about 100 km wide region crossed Transdanubia in the direction of north-west – south-east. The model forecasted the formation of the thunderstorms one hour before the appearance of the first thunderstorm cells. The thunderstorms started to form at about 8 a.m. (UTC),

and cells with large reflectivity were observed until midnight. Although the convective activity significantly decreased after 10 p.m., a few cells were observed even the next morning. The time evolution of the maximum reflectivity and the number of the cells observed with reflectivity larger 45 dBZ are presented in *Table 1*. The maximum reflectivity was higher than 50 dBZ until 20:30. Large number of cells were observed in the morning between 9:30 and 10:30 and in the evening between 18:30 and 20:30. While the first maximum of the convective activity was the consequence of the approaching convergence line, the second maximum was due to the cold front.

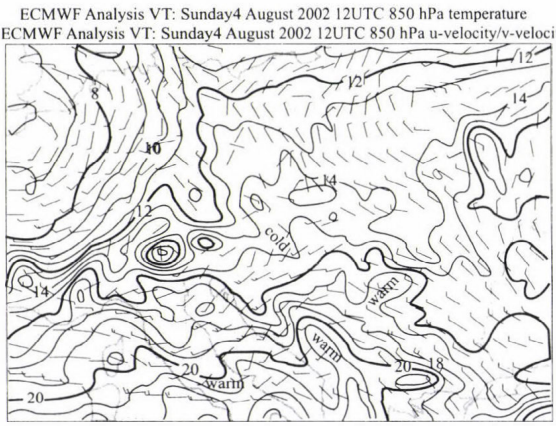

Fig. 2e. 850 hPa temperature and wind fields at 12:00 UTC, August 4, 2002. Thunderstorms of the prefrontal squall line decreased the temperature gradient of the cold front.

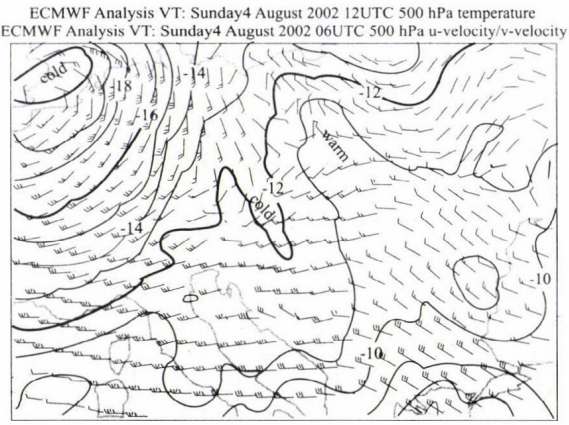

Fig. 2f. 500 hPa temperature and wind fields at 12:00 UTC, August 4, 2002. The high level cold trough of the prefrontal squall line is well separated from the main western cold air mass.

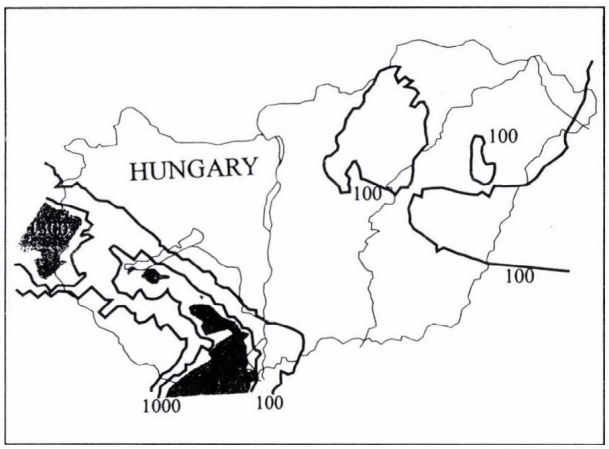

Fig. 3. CAPE calculated by the nowcasting system for the forecast of thunderstorm formation. This figure was released at 10:00 UTC, August 4, 2002. The numbers at the isolines denote the value of CAPE. The dark areas denote the region where the CAPE is larger than 1300 J/kg.

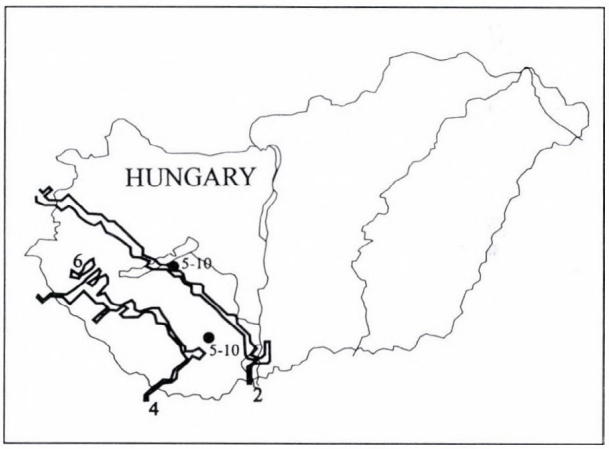

Fig. 4. Isolines of the maximum hailstone size at 10:00 UTC. The numbers at the isolines denote the diameter of the largest hailstones that could reach the ground. The black dots denote the places of the hail reports this day. The numbers at the black dots mean the observed size of the hailstones.

In the last column the reported maximum hailstone sizes are given. It is embarrassing that in spite of high reflectivity observed by S-band radar, only a few hail reports were sent this day. This discrepancy questions the applicability of the voluntary reports for verification of the model results. Comparison of

hailpad and radar observation shows that possibility of hail on the surface is large if the reflectivity is over 55 dBZ (*Dye* and *Martner*, 1978). The calculated maximum hailstone size (third column in *Table 1*) correlates well with the measured maximum reflectivity. (The model gives the maximum hailstone size in different size categories to make the comparison easier between model results and observations.) The isolines of the forecasted maximum hailstone sizes are also involved in the outputs of the nowcasting system (*Fig. 4*). (Note, that hailstone is defined as a bulk ice particle larger than 5 mm, the smaller ones are considered graupel particles.) The numbers next to the dots in this figure denote the reported hailstone sizes in mm. Although these data agree well with the calculated values, the verification of the output for the hailstone size needs more observations.

Table 1. Comparison of model results and observations on August 4, 2002. The first column gives the time in UTC. In the fifth column the number of cells with maximum reflectivity larger than 45 dBZ is given. d_{max} denotes the calculated and observed maximum hailstone size

Time	Model results		Observation		
	Thunder-storm	d_{max} (mm)	Max. refl. (dBZ)	N (cells)	d_{max} (mm)
7:30	yes	5 – 10	34.0	0	–
8:30	yes	5 – 10	45.0	1	–
9:30	yes	5 – 10	58.0	11	5 – 10
10:30	yes	10 – 30	55.0	10	5 – 10
11:30	yes	10 – 30	59.0	5	–
12:30	yes	10 – 30	52.0	5	–
13:30	yes	10 – 30	52.0	3	–
14:30	yes	10 – 30	57.0	1	–
15:30	yes	10 – 30	58.0	3	–
16:30	no	5 – 10	50.0	2	–
17:30	yes	5 – 10	53.0	4	–
18:30	yes	5 – 10	59.0	9	–
19:30	yes	5 – 10	54.0	12	–
20:30	yes	5 – 10	54.0	9	–
21:30	yes	5 – 10	54.0	7	–
22:30	yes	3 – 5	47.0	3	–
23:30	yes	3 – 5	39.0	0	–
0:30	no	–	43.0	0	–
1:30	yes	3 – 5	41.0	0	–
2:30	yes	3 – 5	37.0	0	–
3:30	yes	3 – 5	37.0	0	–
4:30	yes	–	43.0	0	–
5:30	yes	–	43.0	0	–
6:30	yes	–	48.0	1	–
7:30	no	–	44.0	0	–
8:30	no	–	45.0	2	–
9:30	no	–	40.0	0	–
10:30	no	–	42.0	0	–
11:30	no	–	29.0	0	–
12:30	no	–	31.0	0	–

Structure of the radar reflectivity pattern (*Fig. 5*) shows similarity to that of calculated CAPE. The direction of the band is similarly north-west – south-east, however, the cells characterized by high reflectivities lie about 50 km north of the calculated CAPE isolines. It is surprising that in spite of the very large value of the CAPE, no radar echoes were observed in southern part of Transdanubia, and low values of reflectivity were observed at the Hungarian-Austrian border. This disagreement emphasizes the importance of the initialization. It is strongly believed that the large values of the CAPE in the cloud free region are the consequence of the incorrect surface data. The check of the possible reasons needs further research.

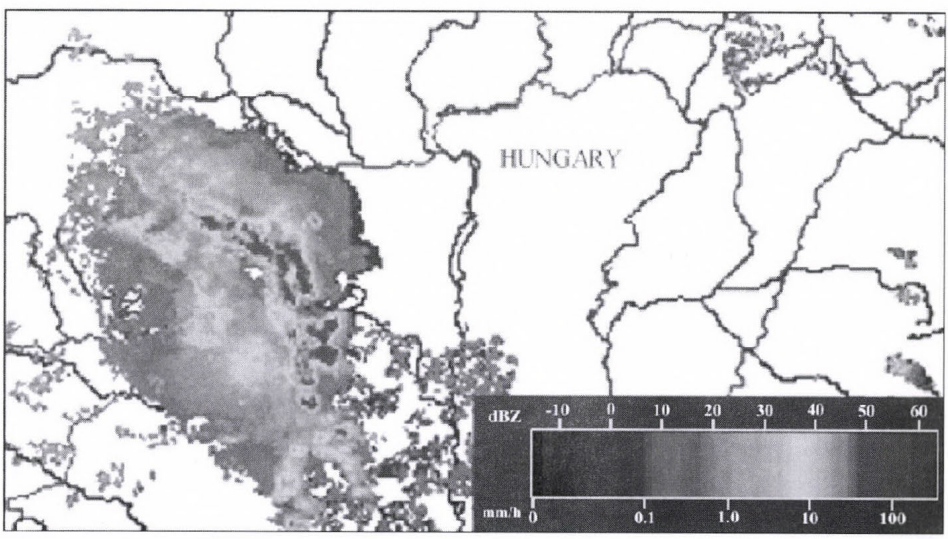

Fig. 5. Radar observation at 10:00 UTC.

5. Verification of model results

The content of *Tables 2* and *3* summarizes the comparison between the observation, based radar measurement and surface report of hail, and model results. The data were gathered over the whole season, between May 1 and September 30, 2002. The nowcasting system sent a report in every hour. These reports contained the warning of the thunderstorm formation and the maximum hailstone size could occur. The nowcasting system issues thunderstorm warning if one of the radars of the Hungarian Meteorological Service detects a thunderstorm cell, and the calculation of the cell movement

(see details in *Horváth* and *Geresdi*, 2003) predicts the appearance of the thunderstorm over the target area. This kind of the thunderstorm forecasting could be unreliable in the case of formation of the airmass thunderstorms. This type of thunderstorms rarely produces large hail, but because of the slow movement, it can result in flood.

Table 2. Observations versus model results for one hour forecast of the thunderstorms

Model	Observations	
	Yes	No
Yes	288	277
No	102	3075

Table 3. Observations versus model results for one hour forecast of the maximum hailstone size

Model	Observations	
	Yes	No
Yes	38	440
No	6	3188

Between May 1 and September 30 the maximum radar reflectivity was larger than 45 dBZ on 61 days. From these days the nowcasting system issued thunderstorm warning on 56 days, that is the system missed the forecast of thunderstorm on six days. Additional analysis of radar observation shows that although the maximum reflectivity was larger than 45 dBZ on these days, the structure of the radar pictures were very similar to that of stratified layer clouds, sometimes with weak embedded convective cells. That means that the nowcasting system forecasts the thunderstorm formation with high reliability on the days when environmental conditions promote this process. However, number of the days with thunderstorms was overestimated by the nowcasting system. Although thunderstorms were not observed by radar over the southern part of the Transdanubia, thunderstorm warning was issued on additional 15 days. This relatively larger ratio (about 25%) could be the consequence of the dissipation of the storm cells before they could reach the target area.

A more detailed analysis of the reports is presented in *Table 2* and in *Table 3* 3672 reports were sent by the nowcasting system during the season.

As *Table 2* shows, the formation of thunderstorm was forecasted 1 hour before the thunderstorms appeared over the target area on 288 occasions. False alarms were sent on 277 occasions. About two third of these reports was sent when the intensity of the thunderstorms decreased as they approached the target area (the maximum reflectivity decreased below 45 dBZ). This situation can be observed between 23:30 and 4:30 in *Table 1*. The convective cells were observed by the radar out of the target area, but their intensity gradually decreased as they approached the target area.

The remaining one third of the reports were released when due to the low activity of the convective cells, they completely dissipated before they reached the target area, or the propagation speed was not calculated correctly. This later case frequently occurred when the convective cells formed in airmass. The missing of the alarm on 102 occasions could be critical. As it is mentioned in the paragraph above, detailed analysis of the radar pictures shows that these situations mostly occurred when the clouds became stratified, and sometimes the maximum reflectivity increased slightly above the threshold value (see, e.g., report at 8:30 in *Table 1*).

Comparison of the hailstone size calculated by the model with that of reported by voluntary observers concludes that the model overestimates both the maximum size and frequency of hail occurrence (*Table 3*). However, as it was mentioned in the case study, we believe that these reports could not be considered to be representative. So further research is necessary for verification of the maximum hailstone size forecast.

6. Conclusion

The numerical model proved to be a useful tool for nowcasting of thunderstorm formation. As the case study showed, the shape of calculated CAPE field is very similar to the radar picture. However, it is not clear why no thunderstorm formation occurred in the southern part of Hungary and near the Austrian-Hungarian border, although the calculated instability was quite large in these regions. One possible explanations may be the inconsistency in the objective analysis between the hourly refreshing surface data and the higher levels forecasted fields which are predicted from the 00 UTC objective analysis. The coupling between the measured surface and forecasted upper level fields can produce physically deformed vertical profiles, when the calculated parameters differ considerably from that of the real atmosphere. The inadequate simulation of the dynamics of squall line could be another reason of the overestimation of the area where intensive thunderstorms formed. (The applied mesoscale model is a hydrostatic model.) In the future, a non-

hydrostatic numerical model is intend to be used, and also a more frequent (about in every 3rd hour) run of the model is planned to give the necessary initial parameters for nowcasting system. The case study shows that if the MEANDER forecasts the convective activity only on the base of calculated CAPE values, the frequency of the thunderstorm formation would be overestimated. The number of these false warnings are reduced by taking into consideration the earlier radar observations. Unfortunately this technique is not efficient in the case of the slowly moving airmass thunderstorms and for longer time period.

The contingency tables show that the reliability of the nowcasting system is high for one hour forecast, but considering the two or three hours forecast, the ratio of the false alarms gets larger.

Although the calculated maximum hailstone sizes correlate well with the large reflectivity values measured by the radar, the comparison with surface hail reports shows that the model significantly overestimates both the frequency of hail occurrence and the maximum hailstone size. This could be the consequence of the very simple model dynamics, and also the neglect of the collision between the water drops and hailstones in the precipitation shaft may lead to the overestimation of the maximum hailstone size. However, the comparison of the radar observations and the surface hail reports allows us to suspect that the reliability of these reports is questionable. The hailpad network, applied during the 80's, may be a more efficient way for surface observation of hailstones (*Székely* and *Zoltán*, 1984).

Acknowledgements—The authors are grateful to Nefela South Hungarian Association for Hail Suppression for providing the radar data and hail reports. The research was supported by the Hungarian Scientific Research Fund (T043010).

References

Aleksic, N., Nikolic, I., and *Jovanovic, D.*, 1991: Forecasting of convective activity using a one-dimensional steady-state cloud model. *Month. Weather Rev. 119*, 3099-3103.

Anthens, R.A., 1977: A cumulus parametrization scheme utilizing a one-dimensional cloud model. *Month. Weather Rev. 105*, 270-278.

Colle, B.A. and *Clifford F.M.*, 2000: The 5-9 February 1996 Flooding Event over the Pacific Northwest: Sensitivity Studies and Evaluation of the MM5 Precipitation Forecasts. *Monthly Weather Review 128*, 593–617.

Foote, G.B. and *Mohr, C.G.*, 1979: Results of a randomized hail suppression experiment in Northeast Colorado. Part VI: Post Hoc stratification by storm intensity and type. *J. Appl. Meteor. 18*, 1589-1600.

Frankhauser, J.C., 1988: Estimates of thunderstorm precipitation efficiency from field measurements in CCOPE. *Month. Weather Rev. 116*, 663–684.

Dessens, J., 1986: Hail in Southwestern France. II: Results of a 30-year hail prevention project with silver iodide seeding from the ground. *J. Climate Appl. Meteor. 25*, 48-58.

Dye, J.E. and *Martner B.E.*, 1978: The relationship between radar reflectivity factor and hail at the ground for northeast Colorado thunderstorms. *J. Appl. Meteor. 17*, 1335-1341.

Geresdi, I. and *Horváth, Á.*, 2000: Nowcasting of precipitation type. Part I: Winter precipitation. *Időjárás 104*, 241-252.

Horányi, A., *Ihász, I.*, and *Radnóti, G.*, 1996: ARPAGE/ALADIN: A numerical weather prediction model for Central-Europe with the participitation of the Hungarian Meteorological Service. *Időjárás 100*, 277-301.

Horváth, Á. and *Geresdi, I.*, 2000: Severe convective storms and associated phenomena in Hungary. *Atmospheric Research 56*, 127-146.

Horváth, Á. and *Geresdi, I.*, 2003: Severe storms and nowcasting in the Carpathian Basin. *Atmospheric Research 67-68*, 319-332.

Marwitz, J.D., Middleton, J.R., Auer, Jr., A.H., and *Veal, D.L.*, 1970: The dynamics of updraft vaults in hailstorm as inferred from the entraining jet model. *J. Atmos. Sci. 27*, 1099-1102.

Pielke, R.A., Cotton, W.R., Walko, R.L., Tremback, C.J., Lyons, W.A., Grasso, L.D., Nicholls, M. E., Moran, M.D., Wesley, D.A., Lee, T.J., and *Copeland, J.H.*, 1992: A comprehensive meteorological modeling system – RAMS. *Meteorol. Atmos. Phys. 49*, 69-91.

Pruppacher, H.R. and *Klett, J.D.*, 1997: *Microphysics of Clouds and Precipitation*. Kluwer Academic Publisher.

Rasmussen, R.M. and *Heymsfield, A.J.*, 1987a: Melting and shedding of graupel and hail. Part I: Model physics. *J. Atmos. Sci. 44*, 2754-2763.

Rasmussen, R.M. and *Heymsfield, A.J.*, 1987b: Melting and shedding of graupel and hail. Part II: Sensitivity study. *J. Atmos. Sci. 44*, 2764-2782.

Rasmussen, R.M., Levizzani, V., and *Pruppacher, H.R.*, 1984: A wind tunnel and theoretical study on the melting behavior of atmospheric ice particles. Part III. Experiment and theory for spherical ice particles of radius < 500 μm. *J. Atmos. Sci. 41*, 381-388.

Székely, Cs. and *Zoltán, Cs*, 1984: The hailpad possibilities of its usefulness. *Időjárás 88*, 32-45.

Zoltán, Cs. and *Geresdi, I.*, 1984: A one-dimensional steady-state jet model for thundercloud. *Időjárás 88*, 21-31

IDŐJÁRÁS

Quarterly Journal of the Hungarian Meteorological Service
Vol. 108, No. 1, January–March 2004, pp. 51–63

Implementation of CO_2 Q band line mixing computations into line-by-line atmospheric radiative transfer codes

Ferenc M. Miskolczi*[1] and **Martin G. Mlynczak[2]**

[1]*Analytical Services & Materials Inc.,*
One Enterprise Parkway, Suite 300 Hampton, VA 23666, U.S.A.
E-mail: f.m.miskolczi@larc.nasa.gov

[2]*NASA Langley Research Center, Mail Stop 420, Hampton, VA 23681-2199, U.S.A.*

(Manuscript received March 24, 2003; in final form February 12, 2004)

Abstract—In this paper, we discuss the computational difficulties of merging line-mixing models into line-by-line computations. We present the technical details of the upgrade of the High-resolution Atmospheric Radiative Transfer Code (HARTCODE) into an accurate reference line-by-line code for line mixing computations in the Q branches of the CO_2. The implementation of line mixing was based on the model, database, and software that were developed at the Laboratoire de Physique Moleculaire et Applications (LPMA), and the HITRAN2K database absorption line compilation. In the recent version of the line mixing database 306 vibrational bands of eight CO_2 isotopes are included, and there are provisions for calculations using the first order and the more accurate relaxation operator method. The successful integration of the line mixing computations has been validated using airborne and ground-based high-resolution HIS radiance measurements. This exercise can also be regarded as the validation of the line mixing database for high resolution, nadir viewing thermal emission measurements.

Key-words: HITRAN, line mixing, HARTCODE.

1. Introduction

According to comparisons of the high-resolution spectral radiance simulations with measurements, ignoring the CO_2 Q band line mixing effects could be responsible for errors of about 20 per cent in the computed outgoing long wave spectral radiance (*Haskins et al.*, 1999). Line mixing is a term to describe the effect of the pressure on the closely packed absorption lines belonging to the same

* Corresponding author. Tel: 757-827-4627; Fax: 757-825-8659

vibrational band. Whenever the line spacing is comparable to the pressure broadened half width, the lines will overlap and collision will broaden and mix the lines creating interference terms in the band shape. More detailed theoretical description and quantitative analysis of line mixing can be found in the literature, see for example *Armstrong* (1982).

Here we shall focus only on the technical details of how line mixing may be implemented into a line-by-line (LBL) atmospheric radiative transfer code. In particular, how the LPMA line mixing model (*Rodriguez et al.*, 1999; *Jucks et al.*, 1999) was implemented into the HARTCODE (*Miskolczi et al.*, 1990; *Rizzi et al.*, 2002).

The size of the most recent version of the LPMA distribution archive is about 17 MB (un-compressed), representing the situation of the database in May 2002. In the database the absorption line and line mixing parameters of 18708 CO_2 Q lines in the 468–6936 cm^{-1} spectral range are organized into 918 files. The structure of the archive is very clear and compact, see *Fig. 1*. The SOFT_Q directory contains software that is ready for use for any homogeneous CO_2 path. In DATA_Q the BANDINF.DAT file gives a summary of the included vibrational transitions. Files S_1... S_{306}, Y_1... Y_{306}, and W_1... W_{306} are the spectroscopic information, first order line mixing coefficients, and the elements of the relaxation operator, subsequently. The TEST_Q directory contains precomputed cases for the consistency check of the full database. The sub-branches of the asymmetric CO_2 molecules are treated as separate bands. The number of the 'true' Q branches is 271. The LPMA database and software are not optimized for LBL radiative transfer computations in the atmosphere.

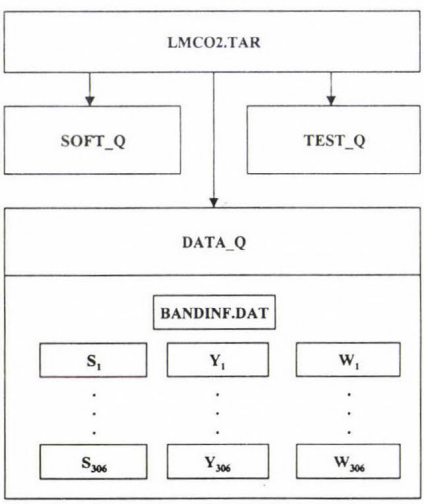

Fig. 1. Structure of the LPMA CO_2 Q band line mixing archive.

HARTCODE is a general purpose software for optical depth, transmittance, radiance, and flux density computations in a spherically stratified refractive atmosphere using the LBL method. The schematic diagram of the code is presented in *Fig. 2*. The LAYER–1 section processes the input atmospheric profile and may output details of the slant path, layering, and viewing geometry. The spectral quantities are read in the wave number loop, and this is the place where line mixing parameters will enter. LAYER–2 module computes the monochromatic optical depth over an appropriate wavenumber grid which is necessary for the wavenumber integration. This part of HARTCODE has been substantially modified to accommodate line mixing computations. In the LAYER–3 module the spectral mean quantities of the output parameters are computed for any required viewing geometry. HARTCODE uses a unique input absorption line file, which is prepared by a preprocessing code. This file is shaped for fast and efficient use with a given radiative transfer problem.

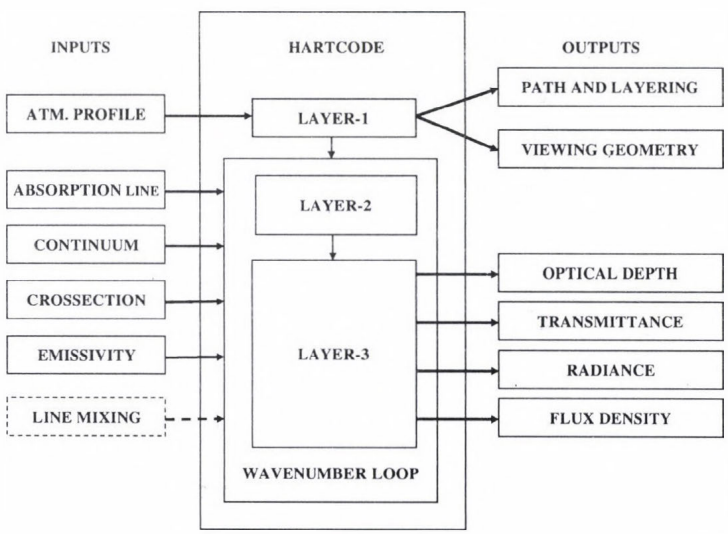

Fig. 2. Schematic structure of the High-resolution Atmospheric Radiative Transfer Code.

In this work the input absorption lines were taken from the HITRAN2K database (*HITRAN2K,* 2002). This compilation contains over a million transitions of 38 different absorbers, but the CO_2 Q lines are identical to those of present in the 1996 edition (*Rothman et al.*, 1998). The HITRAN2K database contains several improvements, among others, improved water vapor line parameters, which are important when comparing simulated and measured radiance spectra.

Regarding the CO_2, we have altogether 60802 transitions, out of these 11694 are Q lines of 328 Q bands. Although, in its original form, the HITRAN2K absorption line file is suitable for line-by-line computations, for efficient use, and for line mixing computations it must be re-shaped.

Implementation of line mixing into HARTCODE was taken in two steps. First the LPMA and HITRAN2K databases were treated to make them suitable for direct HARTCODE access. Next, the subroutines to compute line-mixing with the first order or the relaxation operator method were added, together with the necessary changes in some existing HARTCODE modules.

2. Modifications related to the LPMA and HITRAN2K databases

In HARTCODE the grid structure for wave number integration over a given resolution is non-uniform, and is set up by using the absorption line positions present in the input line file. The LPMA and HITRAN2K databases were created by using different sources of theoretical and experimental spectroscopic data, therefore, the first step was to solve line compatibility problems between the two databases. HITRAN2K contains several Q bands which are not included in the LPMA, while most of the coincidental Q bands contain more absorption lines in the LPMA than in the HITRAN2K. In *Fig. 3* the absorption lines in the coincidental Q bands are plotted in the 500–1000 cm^{-1} spectral range. Apparently, most of the excessive LPMA Q lines are weak. In case the wave number grid points are generated using the HITRAN2K lines, grid points would be missing for these weak lines. On the other hand, merging thousands of very weak LPMA Q lines into the input line file would introduce unnecessary computational burden, which should be avoided. However, the line mixing computation of the monochromatic absorption coefficient requires all rotational lines of a given vibrational transition that were included in the development of the LPMA parameterization.

The simple practical solution to the above problem is to use two properly organized and filtered data files. The first one is an ordinary line file which contains all transitions of all absorbers that have significant contributions to the absorption coefficients. Also, it should contain a kind of complex flag which identifies the Q bands for which line mixing coefficients are available in the LPMA database. This first file will control the setup of the wavenumber grid. The second file contains all LPMA Q lines and the line mixing coefficients sequentially organized into blocks by the minimum wave number of the rotational lines in the contributing vibrational bands. To create these two files, the HARTCODE line preprocessing software was modified. The modified code is performing the following tasks:

- Checks the original HITRAN2K data file for unhandled transitions.
- Determines the coincidental Q bands and marks the related transitions.
- Re-organizes the LPMA database into a blocked sequential file.
- Merges the LPMA database to the HITRAN2K.
- Applies filters on the combined database and creates the final line file.

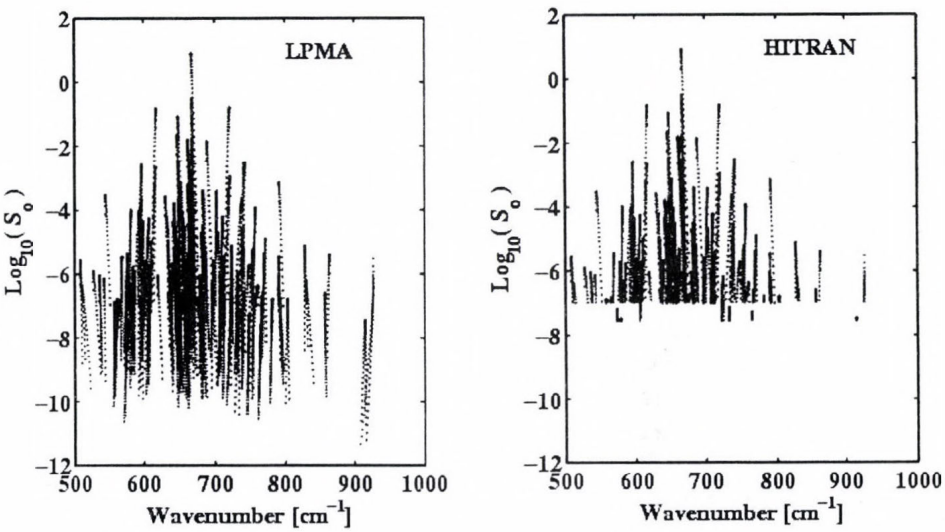

Fig. 3. Intensity distributions of the LPMA and HITRAN2K Q lines in the coincidental Q bands. S_o [cm^{-1} (atm-cm$_{STP}$)$^{-1}$] is the line intensity at 296 K.

As an example of the operation of the pre-processing code, some numerical results for a spectral radiance simulation problem in the 450–3550 cm^{-1} spectral range, using a vertical path trough the whole USS 76 atmosphere are given. In this case the filters were set to keep only those transitions which contribute more than 10^{-2} per cent to the total Voigt monochromatic absorption coefficients at the line centers. As a result, there remained 98994 transitions in the final absorption line file (with 21336 CO_2 and 8740 coincidental CO_2 Q lines), and 11968 transitions in the LPMA line mixing file. Ten other molecular species, H_2O, N_2O, CO, CH_4, O_2, NO, SO_2, NO_2, and N_2 were also contributing to the final number of transitions. These line files were used at the validation of the line mixing model with the High-resolution Interferometer Sounder (HIS) measurements.

In case of interest, a complete set of five FORTRAN line processing routines are available from the authors. These codes may be used to process the LPMA database with the different HITRAN editions or other absorption line archives.

3. Modifications in HARTCODE

Major modifications of the HARTCODE were needed for two reasons. Firstly, the nature of the computation of the line mixing with the first order or relaxation operator method requires the interruption of the strict sequential reading of the input absorption line file, and jump into a reading sequence, based on the positions and widths of the vibrational bands. Since Q bands have complex overlapping structure, the treatment of the ordinary lines and the marked Q lines is rather complex. Secondly, the mathematical representations of the line mixing computations require the efficient evaluation of the complex probability function and library routines for handling complex operators. A summary of the equations relevant to the line mixing computations is given in the Appendix.

Introducing the line mixing option into the HARTCODE resulted in significant increase of the size of the code. The new version of HARTCODE contains about 1700 more program lines. Eleven subroutines have been added. The first six are performing the following tasks: read the LPMA Q line file; evaluate the complex probability function; compute the transition population, first order line mixing coefficients, Lorentz half widths, and relaxation matrix elements for the current temperature and pressure; compute the absorption coefficients; compute the equivalent Q lines. The other six routines are from the LPMA Mathematical Library and their tasks are to diagonalize and invert complex operators. Some of the above routines are the slightly modified versions of the codes available in the SOFT_Q directory of the LPMA distribution archive. During the implementation major efforts were devoted to resolve the synchronized reading of the two absorption line files and to develop consistent line wing cut–off concept for the coincidental Q lines.

As an illustration, the effect of the code modifications is shown in *Figs. 4* and *5*, where monochromatic layer optical depth computations are compared with- and without applying line mixing. In *Fig. 4* the unmodified code results are presented. In *Fig. 5* the difference between the two curves at the top shows the effect of the line mixing on the total optical depth. The maximum difference is about 50 per cent and it occurs at around 618.5 cm^{-1}. The set of curves at the middle of *Fig. 5* represents the optical depth from the LPMA Q lines, and the bottom set of curves are the contributions from the other molecules and non-LPMA Q lines. Each curve in the sets shows the variation of the optical depth of an atmospheric layer between the altitudes of 0 and 20 km.

The spectral interval has a width of 1.0 cm^{-1} and contains 1332 grid points for the wavenumber integration.

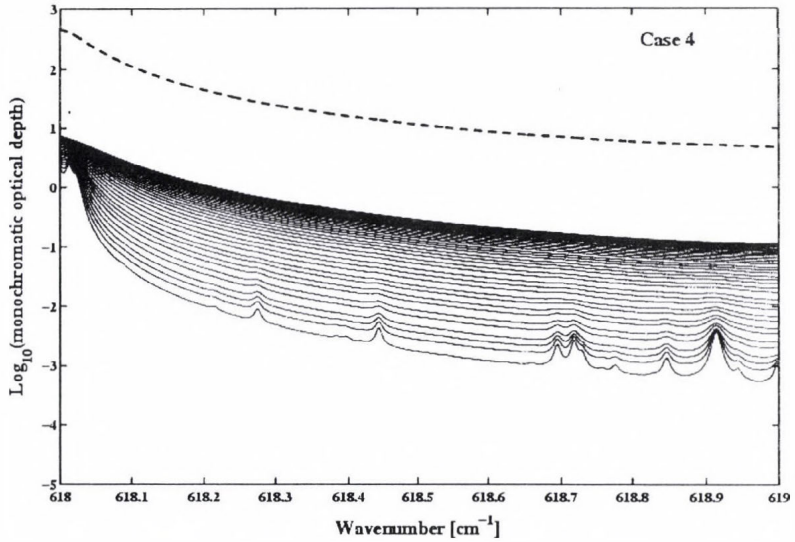

Fig. 4. Monochromatic optical depth of the atmospheric layers at different altitudes. Computed for the UWITRA93 case 4 without line-mixing. Dashed line is the total optical depth through the 20 km vertical path.

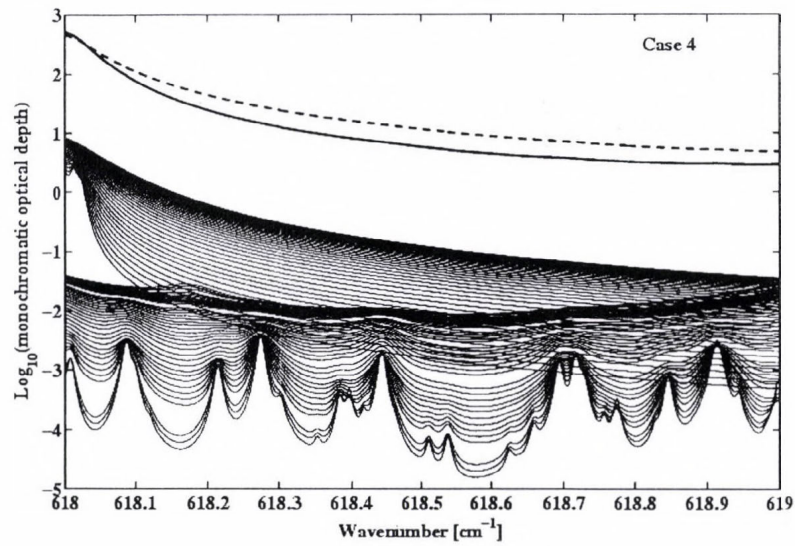

Fig. 5. Monochromatic optical depth of the atmospheric layers at different altitudes. Computed for the UWITRA93 case 4 with line-mixing. The top two lines are the total optical depths with- and without line-mixing. The two set of curves are the results of the separation of the absorption lines into LMPA Q lines and other absorption lines.

4. Validation

To validate the newly implemented line mixing algorithm for atmospheric applications, we selected the UWITRA93 data set (*Knuteson,* 1993). Since HARTCODE was participating in the 1993 ITRA exercise, the atmospheric profiles and the radiance measurements were ready for immediate use, see *Figs. 6* and *7*. In the data set there are two up-looking (ground based), and two down-looking (airborne) measurements. The unapodized spectral resolution of the HIS instrument in the band 1 (600–1080 cm^{-1}) is about 0.3 cm^{-1}. HARTCODE radiances, with- and without applying first order line mixing computations, were computed with 0.005 cm^{-1} spectral resolution. The relative differences in the downward radiances, (cases 1 and 2), are about 20 to 50 per cent, but for Q bands closer to the window region it may exceed 80 per cent, see *Fig. 8*. The line-mixing effects on the upward radiances, (cases 3 and 4), are considerably less, and remain below 20 per cent. This is mainly due to the significant contributions to the radiances from the surface.

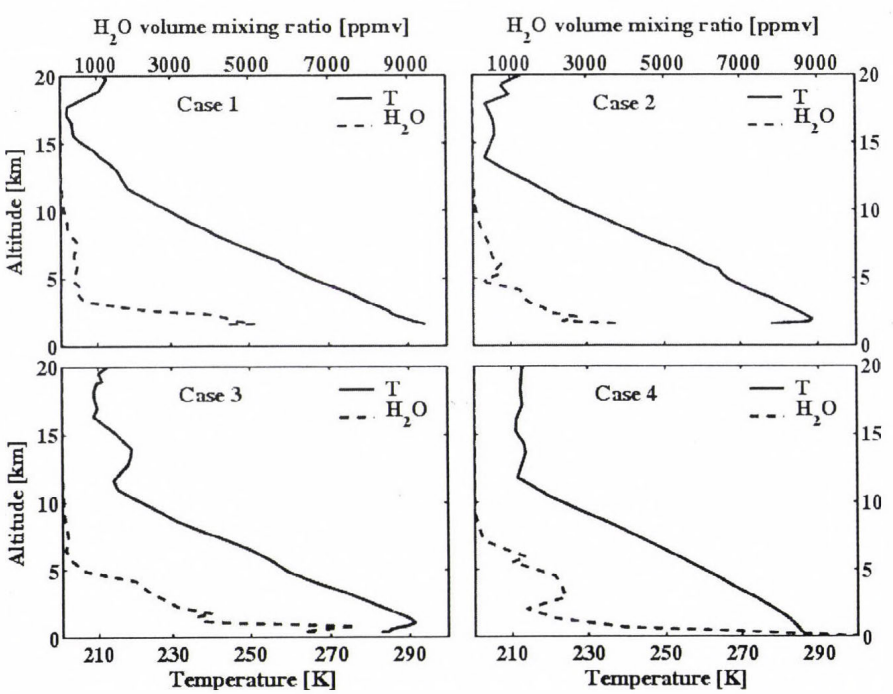

Fig. 6. Temperature and H_2O volume mixing ratio profiles of the UWITRA93 data set. Cases 1 and 2 were used for the ground based HIS simulations and cases 3 and 4 were used for the simulations of the aircraft measurements.

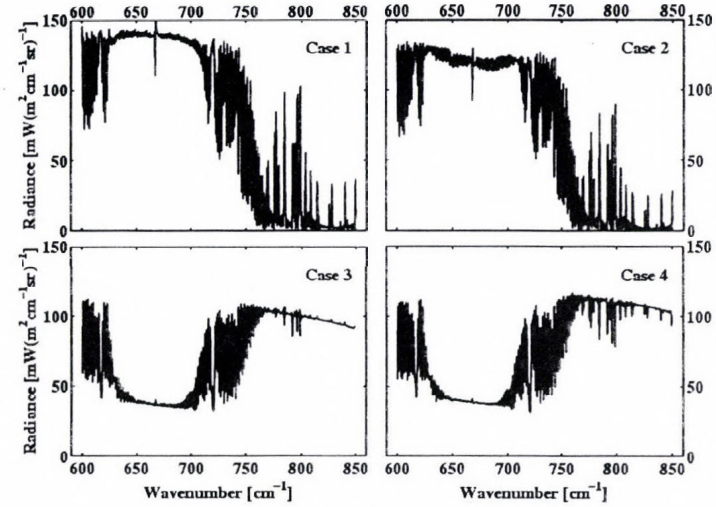

Fig. 7. High-resolution Interferometer Sounder radiance measurement in band I for the UWITRA93 cases. These radiances were used for the validation of the line-mixing model and its implementation into HARTCODE. The spectral resolution is 0.36 cm^{-1}.

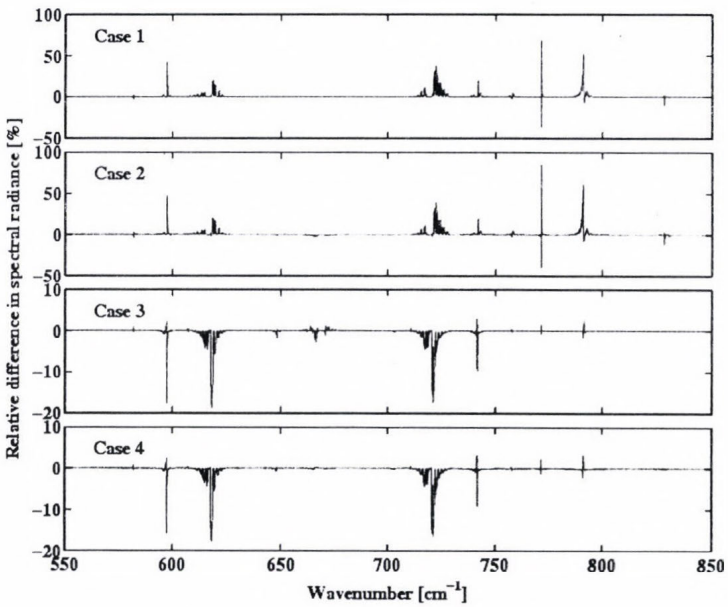

Fig. 8. Effect of line-mixing on the high-resolution simulated spectra. UWITRA93 cases, 0.005 cm^{-1} spectral resolution. The relative difference is defined as $100(R-R_x)/R_x$, where R is the radiance without line-mixing and R_x is with line-mixing.

To model the HIS measurements, the HARTCODE radiances were evaluated using the FFT method, which involves interpolation, smoothing, fast Fourier transform, truncation, zero filling, and inverse Fourier transform. Here we used linear interpolation for 2^{19} discrete wavenumber points. Since unapodized radiances can have zero or negative values, relative errors can not be computed. In *Fig. 9* the differences in the simulated and measured radiances are displayed. The upper curves in case 1 and 2 and the lower curves in case 3 and 4 are the differences without line mixing. The other four curves in the plots (they are vertically offset by +/–10 units for better view) show the differences when the line mixing effect was considered. Here we are not going into the quantitative details of the comparison, our purpose is merely to show that the LPMA line mixing model works properly within HARTCODE. Apparently, there are large improvements by introducing the line-mixing, actually bringing the differences close to the instrument noise. Line-mixing computations with the relaxation operator method produced very similar results, (not shown here), but with considerably longer computing time. Obviously, line mixing computation has a price. The computer time necessary to run a case was increased by a factor of three for the first order method, and a factor of six for relaxation operator method. Note, that one single HARTCODE run in the 450–3500 cm^{-1} spectral range, (with 0.005 cm^{-1} resolution and using 80 atmospheric layers), without line mixing takes about 15 minutes on a 2.8GHz HP PC.

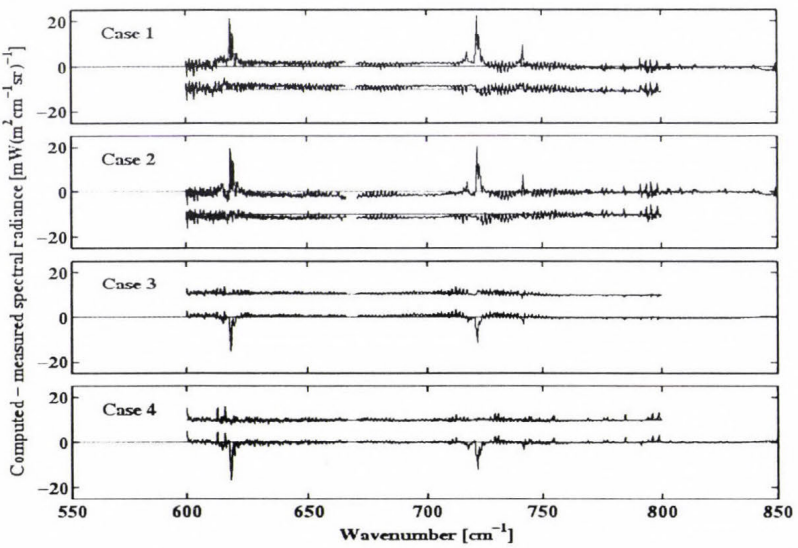

Fig. 9. Effect of line-mixing on the simulation errors. The longer curves in the plots were computed without line-mixing. The shorter curves, with +/–10 units vertical offsets, are the errors when line-mixing was considered in the calculations.

5. *Conclusions*

Here we have demonstrated that the LPMA line mixing model can be effectively implemented and used within a line-by-line atmospheric radiative transfer code. The key to the LPMA data base was to make it suitable for simultaneous sequential processing with the HITRAN2K absorption line file. It appears that the development of an interface code which is unique for the LPMA database, (or for any other line mixing database with different structure), is always necessary. The excellent documentation of the LPMA archive made this job relatively easy. Once this code is developed, the use of further editions of the HITRAN database with different CO_2 lines, or using a new LPMA edition (with better line mixing parameters, but with the same structure) will be a matter of re-running the software. The increased computer time of the LBL calculations has little importance when the accuracy is the primary concern.

The scientific community, engaged with molecular spectroscopy and atmospheric radiative transfer, has long time been awaiting for readily available line mixing parameters and algorithms that are included into the further editions of the HITRAN database. Regarding the number of existing line mixing models and parameterizations, see for example *Hoke et al.* (1994), *Strow et al.* (1994), *Timofejev et al.* (1997), the evaluation, selection, and implementation could take a long time. Meanwhile, as the most recent and most comprehensive CO_2 line-mixing archive, the LPMA model may be used alternatively.

Acknowledgements—We are very grateful to *J. M. Hartmann* for the most recent version of the LPMA line mixing archive and to *R. O. Knuteson* for the HIS measurements and the related documentation.

APPENDIX

Formulas relevant to line-mixing computations

Line intensity definition in HITRAN (in units of cm^{-1} (molecules $cm^{-2})^{-1}$):

$$S_i^0 = \Pi_i(T_0) D_i^2 \nu_i (1 - \exp(-c_1 \nu_i / T_0)).$$

Voigt monochromatic absorption coefficient for non-LPMA Q lines and other CO_2 lines:

$$k_\nu(p,T) = \mathrm{X}_{CO_2} \frac{T_S p}{p_S T} L_0 \sum_{i=1}^{N} S_i^0 \frac{\left(1 - e^{-c_1 \frac{\nu}{T}}\right) F_i(T_0)}{\left(1 - e^{-c_1 \frac{\nu_i}{T_0}}\right) F_i(T)} \sqrt{\frac{\ln 2}{\pi}} \frac{e^{-c_1 E_i \frac{T_0 - T}{T_0 T}}}{c_3 \sqrt{\frac{T}{M_i}} \nu_i} [V(x,y)]^{RE}.$$

First order line mixing absorption coefficient for LPMA Q lines:

$$k_v^F(p,T) = A_v(p,T)\sum_{i=1}^{N} B_v^i(T)\left(\left[V(x,y)\right]^{RE} - Y_i(T)\left[V(x,y)\right]^{IM}\right).$$

Absorption coefficient for the equivalent Q lines:

$$k_v^R(p,T) = A_v(p,T)\sum_{i=1}^{N} \frac{\left([SE_i]^{RE}[V(x,y)_i]^{RE} - [SE_i]^{IM}[V(xx,yy)_i]^{IM}\right)}{c_3\sqrt{\frac{T}{M_i}}},$$

where

and

$$A_v(p,T) = \mathrm{X}_{CO_2}\frac{T_S p}{p_S T}L_0(1-e^{-c_1\frac{v}{T}})\sqrt{\frac{\ln 2}{\pi}},$$

$$B_v^i(T) = \Pi_i(T_0)\frac{F_i(T_0)}{F_i(T)}D_i^2\frac{e^{-c_1E_i\frac{T_0-T}{T_0T}}}{c_3\sqrt{\frac{T}{M_i}}}.$$

List of symbols

$\Pi_i(T_0)$	Population at temperature T_o
D_i	Dipole moment
v_i	Resonance wavenumber, cm^{-1}
c_1	1.4387686
T_0	296.00 K
X_{CO2}	CO_2 volume mixing ratio
T_s	273.15 K
p_s	1013.25 hPa
T	Temperature, K
p	Pressure, hPa
L_o	2.68710×10^{19}
v	Wave number, cm^{-1}
N	Total number of the Q lines of all contributing bands
$F_i(T)$, $F_i(T_0)$	Partition functions of the CO_2 isotope
E_i	Ground state energy
c_3	3.58128×10^{-7}
M_i	Molecular weight of the CO_2 isotope
$V(x,y)_i$	Complex probability function
$x = (v - v_i)(\ln 2)^{1/2}/\alpha_D$	Real part of the argument of V
$y = \alpha_L/\alpha_D(\ln 2)^{1/2}$	Imaginary part of the argument of V
$\alpha_D = c_3(T/M_i)^{1/2}v$	Doppler half width
$\alpha_L = \alpha_o^i(p/p_s)(T_0/T)$	Lorentz half width

Γ	Temperature coefficient of the ith transition
α_o^i	Lorentz half width at T_o and p_s
$xx = (H^R + \nu_i^* - \nu)(\ln 2)^{1/2}/\alpha_D$	Real part of the argument of V for the equivalent lines
$yy = H^I (\ln 2)^{1/2}/\alpha_D$	Imaginary part of the argument of V for the equivalent lines
H^R	Positions of the equivalent lines
H^I	Half width of the equivalent lines
SE_i	Complex intensities of the equivalent lines
ν_i^*	Population-averaged wave number.

The superscripts *RE* and *IM* refers to the real and imaginary part of the V complex probability function and $Y_i(T)$ is the first order line mixing coefficient. The sums in the above equations are extended to all the lines of all contributing Q bands at a particular wavenumber. Detailed explanation of H^R and H^I can be found in *Rodriguez et al.* (1999).

References

Armstrong, R.L., 1982: Line mixing in the ν_2 band of CO_2. *Applied Optics 21*, 2141-2145.

HITRAN2K. 2002; http://cfa-www.Harvard.edu/HITRAN/hitrandata.

Haskins, R., Goody, R., and *Chef, L.*, 1999: Radiance covariance and climate models. *J. Climate 12*, 1409-1422.

Hoke, M. L., Clough, S.A., Kneizys, F.X., and *Anderson, G.P.*, 1994: Line coupling in fifteen micron carbon dioxide Q-branches: Review and implementation in FASCOD3. *Proc. SPIE 2309*, 170-183.

Jucks, K. W., Rodriguez, R., LeDoucent, R., Claveau, C., Traub, W.A., and *Hartmann, J.M.*, 1999: Model, software, and data-base for computation of line-mixing effects in infrared Q branches of atmospheric CO_2. II. Minor and asymmetric isotopomers. *J. Quant. Spectros. Radiat. Transfer 63*, 31-48.

Miskolczi, F., Bonzagni, M., and *Guzzi, R.*, 1990: High resolution atmospheric radiance - transmittance code (HARTCODE). In *Meteorology and Environment Sciences: Proc. of the Course on Physical Climatology and Meteorology for Environmental Application*. World Scientific Publ. Co. Inc., Singapore, 743-790.

Rodriguez, R., Jucks, K.W., Lacome, N., Blanquest, G., Valrand, J., Traub, W.A., Khalil, B., LeDoucent, R., Valentin, A., Camy-Peyret, C., Bonamy, L., and *Hartmann, J.M.*, 1999: Model, software, and data-base for computation of line-mixing effects in infrared Q branches of atmospheric CO_2. I. Symmetric isotopomers. *J. Quant. Spectros. Radiat. Transfer 61*, 153-184

Rizzi, R., Matricardi, M., and *Miskolczi, F.*, 2002: Simulation of uplooking and downlooking high-resolution radiance spectra with two different radiative transfer models. *Applied Optics 41*, 940-956.

Rothman, L.S., Rinsland, C.P., Goldman, A., Massie, T., Edwards, D.P., Flaud, J.-M., Perrin, A., Camy-Peyret, C., Dana, V., Mandin, J.-Y., Schroeder, J., Cann, A., Gamache, R.R., Wattson, R.B., Yoshio, K., Chance, K.V., Jucks, K.W., Brown, L.R., Nemtchinov, V., and *Varansi, P.*, 1998: The HITRAN molecular spectroscopic database and HAWKS (HITRAN atmospheric workstation): 1996 edition. *J. Quant. Spectrosc. Radiat. Transfer 60*, 665-710.

Strowe L.L., Tobin D.C., and *Hannon S.E.*, 1994: A compilation of first-order line-mixing coefficients for CO_2 Q-branches. *J. Quant. Spectrosc. Radiat. Transfer 52*, 281-294.

Timofejev Y.M., Polyakov A V., Tonkov M.V., and *Filippov N.N.*, 1997: Line-mixing influence on the slant path transmittance and limb atmospheric radiation in different IR absorption bands. IRS'96: Current Problems in Atmospheric Radiation. *Proc. of IRS'96*, Fairbanks, Alaska, USA, 1004-1007.

IDŐJÁRÁS

Quarterly Journal of the Hungarian Meteorological Service
Vol. 108, No. 1, January–March 2004, pp. 65–75

Aerodynamic properties of air layer above maize canopy during windy conditions

Taťjana Hurtalová[1], František Matejka[1], Blanka Chalupníková[2] and Jaroslav Rožnovský[3]

[1]*Geophysical Institute of the Slovak Academy of the Sciences, Dúbravská cesta 9, 845 28 Bratislava 45, Slovak Republic; E-mail: geoftahu@savba.sk*

[2]*Czech Hydrometeorological Institute, Kroftova 43, 616 67 Brno, Czech Republic; E-mail: chalupnikova@chmi.cz*

[3]*Department of Landscape Ecology, Mendel University of Agriculture and Forestry, Zemědělská 1, 613 00 Brno, Czech Republic; E-mail: roznovsky@chmi.cz*

(Manuscript received April 5, 2002; in final form February 7, 2003)

Abstract—The analysis of the wind speed profile measurements carried out above maize canopy during the whole growing season were used for dependence parameterization of the dynamic roughness length z_0 as well as aerodynamic resistance r_a on the wind speed $u(z)$. The investigated experimental field is situated in Žabčice, Czech Republic (49°01'N, 16°37'E, 179 m a.s.l.). The zero plane displacement d, the roughness length z_0, and the aerodynamic resistance r_a values were determined during the whole maize growing season. On the basis of these values, the dependence of the z_0 and ra values on the wind speed was found and quantitavely expressed for this canopy surface. For zero plane displacement d we accepted the fact, that the relation $d = (2/3)h$ is well representative for agricultural crop covered surfaces. The average roughness length of closed maize canopy was from 0.24 m in August to 0.19 m in October with mean canopy height of 2.24 m and 2.15 m, respectively. The dependence of friction velocity u^* on the wind speed $u(0.5\ \mathrm{m})$ can be fitted as $u^* = 0.62[u(0.5\,\mathrm{m})]^{0.69}$. The function $z_0 = f(u)$ can be analyzed as the dependence of the relative roughness length $\xi_0 = z_0/h$ on the nondimensional speed $\Gamma = u(h)/u^*$. For this dependence the analytical relationship was found in the form: $\xi_0 = 0.162 \exp(-0.306\,\Gamma)$. The aerodynamic resistance decreases with increasing wind speed. This dependence is more complicated, because the r_a-values depend also on the rougness length and atmosphere's thermal stratification.

Key-words: wind speed profile, friction velocity, roughness length, zero plane displacement, aerodynamic resistance, maize.

1. Introduction

A coupling of the airflow and the canopy surface takes place above a flexible vegetation during windy conditions. This builds up the waving form of the canopy surface in addition to producing streamlining and fluttering phenomena. Consequently, it may be estimated that the aerodynamic properties vary with the wind speed. This is one of the most striking phenomena of the airflow above a surface formed by vegetation (*Brutsaert,* 1982; *Hayashi,* 1983).

In the analysis of wind structure in the lowest layers of the atmosphere, it is advantageous to regard some horizontal layers where individual relationships of physical amount are established. The surface boundary layer is defined as the lower friction layer, in which the wind structure is strongly influenced by the surface morphologic and thermal conditions. In addition to this fact, it is possible to observe the formation of a new boundary layer generated under the surface boundary layer, if the surface is covered by vegetation.

So it has been noted, that the values of the roughness length and the zero plane displacement change systematically with the wind speed, when they are determined from wind speed profiles measured above a stand of vegetation. Many observations on this phenomenon have been done for different plant canopies (*Saugier* and *Ripley*, 1978; *Hayashi,* 1983; *Mölder,* 1997; *Mölder et al.*, 1999; *Hurtalová* and *Matejka,* 1999). The concept of the roughness length has become a simple and useful tool for parameterization of the surface momentum, sensible heat, and latent heat fluxes (*Brutsaert,* 1982; *Mölder,* 1997). Hence, the roughness length is an important imput parameter in many mathematical models simulating the surface fluxes of mass and energy, as well as in numerical modeling from mesoscale models to long-term climate analyses including general circulation models (*Jasinski* and *Crago,* 1999). Consequently, there is an urgent need to estimate the values of the roughness length for various kinds of earth surfaces with required accuracy and reliability.

The aim of this study was the determination of the zero plane displacement d, the roughness length z_0, and the aerodynamic resistance r_a values during the whole maize growing season. On the basis of these values, the dependence of the z_0 and r_a-values on the wind speed $u(z)$ can be found and quantitatively expressed for this canopy surface.

2. Theory and methods

The generally accepted theory of exchange between the land surface and the lower atmosphere layers is based on the works of *Monin* and *Obukhov* (1953, 1954). With the help of the universal functin $\phi(z/L)$ of Monin-Obukhov, it is

possible to describe the vertical wind speed profile $u(z)$, considering the atmosphere thermal stratification, by relationship

$$\frac{d\overline{u}}{dz} = \frac{u^*}{\kappa z}\phi\left(\frac{z}{L}\right), \tag{1}$$

where u^* is the friction velocity, κ is the Kármán constant, and L is the Monin-Obukhov length. Under neutral conditions, introducing the values of z_0 and d, the vertical wind speed profile is represented by the integrated form of Eq. (1)

$$\overline{u}(z) = \frac{u^*}{\kappa}\ln\left(\frac{z-d}{z_0}\right). \tag{2}$$

Additional basic equations valid in the canopy sublayer are (*Hayashi,* 1983)

$$\tau = \rho K_M \frac{d\overline{u}}{dz}, \tag{3}$$

$$\frac{d}{dz}\left(\frac{\tau}{\rho}\right) = a\, LAD\, C_d \overline{u}^2, \tag{4}$$

$$K_M = \beta \xi_0^{\,m}\, \overline{u} h(1 - rLAD), \tag{5}$$

where K_M is called the eddy exchange coefficient of momentum, $\tau = \rho(u^*)^2$ is the vertical transfer of momentum, ρ is the air density, h is the mean vegetation height, $\xi_0 = z_0 / h$ is the relative roughness length, C_d is the drag coefficient for individual roughness elements, LAD is the leaf area density, r is the luxuriant length, which was defined by *Hayashi* (1983), and a, β, m are nondimensional constants.

Using these relationships and provided that K_M changes continuously and $LAD = 0$ on the level $z = h$, we obtained the relationship for the z_0-values as a function of the nondimensional speed $\Gamma = u_h/u^*$ in the form (*Hayashi,* 1983; *Hurtalová* and *Matejka,* 1999)

$$\frac{z_0}{h} = \xi_0 = \left(\frac{\kappa}{\beta\Gamma}\right)^{\frac{1}{m-1}} \exp\left(\frac{\kappa\Gamma}{m-1}\right), \tag{6}$$

where $m \neq 0$.

The zero plane displacement d can be determined from analysis of the results of the wind speed profile measurements in case of a neutral atmosphere

stratification (*Brutsaert,* 1982). Consequently, in the absence of wind speed profile data at neutral atmosphere stratification, we can use the relationship $d = f(h)$, where h is a mean canopy height increasing during the growing season. The mean of data presented in literature is $d/h = 0.68$, with extremes of 0.53 and 0.83 (*Brutsaert,* 1982; *Mölder et al.,* 1999). Again, it is clear that the ratio d/h also can not really be a constant. But $d = (2/3)h$ appears to be fairly representative for closed vegetation canopy surfaces. The zero plane displacement is the height of the active surface, where the radiation is reflected and transformed into other energy kinds.

The roughness length values can be determined by the analysis of the wind speed profiles measured over an active surface at minimum three levels at different thermal atmosphere stratifications (*Hurtalová et al.,* 1987). Each wind speed profile $u(z)$ can be approximated by the relationship (*Monin* and *Obukhov,* 1954; *Hurtalová et al.,* 1987)

$$u_i(z) = A_i(\gamma + \log(z)) + C_i z\,, \tag{7}$$

where i is the profile number. A_i, γ, C_i are parameters which can be determined by the least squares method for each wind speed profile. Using known values of these parameters, the z_0-values can be estimated by formula

$$z_0 = 10 - \gamma\,. \tag{8}$$

The physical sense of A_i and C_i parameters can be deduced from relationships which are valid for each wind speed profile:

$$u^* = \kappa\, A_i / \ln(10) \quad \text{and} \quad \beta^* / L = C_i \ln(10) / A_i\,, \tag{9}$$

where β^* is Monin-Obukhov's universal semiempirical constant.

The transfer through the canopy air and in the air above it can be represented by an aerodynamic resistance r_a (*Brutsaert,* 1982). The r_a-values can be calculated using simple method on the base of the wind speed profile analysis (*Hurtalová* and *Szabó*, 1985). The aerodynamic resistance to water vapor r_a is defined from relationship (*Brutsaert,* 1982)

$$E = \rho \frac{q_s - q_a}{r_a}\,, \tag{10}$$

where E is the water vapor flux, q_s and q_a are the specific humidity of air at the surface and at the reference height, respectively. Further, let's consider the

definition of the eddy exchange coefficient of momentum K_M (*Hurtalová* and *Szabó,* 1985). For r_a, the relation $r_a = 1/K_M$ is valid. Then, coming out from Monin-Obukhov's theory and considering thermal stratification of the atmosphere for r_a, the following relationship can be found (*Hurtalová,* 1995)

$$r_a = \frac{\ln\left(\frac{z}{z_0}\right) + \frac{\beta^*}{L}(z - z_0)}{\kappa\, u^*}. \tag{11}$$

The atmospheric stratification in Eq. (11) is defined by parameter β^*/L. The values of z_0, u^*, and the parameter β^*/L can be determined by the analysis of the wind speed profiles, according to Eq. (9).

3. Experimental site and data

The experimental site of Žabčice is located in the southern part of Moravia, Czech Republic, in a warm agroclimatological macroregion with a predominantly moderate winter (*Rožnovský* and *Svoboda,* 1995). The average annual temperature is 9.2°C, the average temperature during vegetation season is 15.7°C. The growing season, which is limited by biological zero for maize canopy (8.0°C), in average starts on March 31 and ends on October 20.

The investigated plant species was maize (*Zea maize L.*), for which canopy structure and architecture is changing significantly during the growing season. Plant density was 12 plants/m^2 and row spacing was 0.7 m. The maize "STIRA" variety is middle lateness, two-line hybrid with mark FAO 390. This cultivar is typical one having good economic properties and high harvests, plants are not sensitive to droughts.

The wind speed measurements were part of microclimatic profile measurements above the investigated maize canopy. Anemometers were installed at 0.5 m, 1.0 m, and 2.0 m above the zero plane displacement level on a metallic mast. The values of wind speed were continuously measured by automatic measuring equipment with data logger and anemometers A100L in 15-minute intervals of measurements. For the analysis we selected the wind speed hourly average values, which fulfilled the condition $u(0.5\,\mathrm{m}) \geq 1.0$ m s^{-1}. From this it follows the assumption, that we analyzed the vertical wind speed profiles under the conditions of turbulence development. It can be expected that the shape of a wind speed profile depends on the value of the mean wind speed at level close to canopy height (*Matejka et al.,* 2001).

The analyzed wind speed profiles were measured from May 10 to October 18, 2000. The year 2000 was very dry during the growing season, namely in April the monthly sum of precipitation was altogether 1.6 mm, and during the first part of May (till May 17) it rained only 7.8 mm (*Rožnovský et al.*, 2000). This fact definitely influenced plant growth and development, as well as the closing of maize canopy.

4. Results and discussion

The vertical wind speed profiles, measured in and above maize canopy during the whole growing season fulfilling the condition $u(0.5\text{m}) \geq 1.0$ m s^{-1}, were analyzed. This analyzed series contained 1255 hourly mean wind speed profiles measured from May 10 to October 18, 2000.

As it was mentioned above, April was very dry and this fact importantly influenced the plant growth and structure of maize canopy, namely at the beginning phase of maize. In May the experimental field formed only a bare soil surface. At the end of June this surface was covered by the maize canopy with leaf area index LAI $\sim$ 2.0 m^2 m^{-2}. The surfacewas covered by closed maize canopy, LAI $>$ 3.0 m^2 m^{-2}, from the end of July. The maximum height of the closed maize canopy reached the 2.32 m.

Only few analyzed profiles were measured in neutral atmosphere stratification. Therefore we accepted the fact, that relation $d = (2/3)h$ is good representative of agricultural crop covered surfaces (*Brutsaert,* 1982; *Mölder et al.*, 1999).

Seasonal course of daily average values of canopy height h and $(d+z_0)$ is indicated in *Fig. 1*. It is known, that the roughness length is dependent on the canopy structure and architecture, as well as on the wind speed. Therefore, the dependence of z_0-values on the wind speed will be analyzed above closed maize canopy (August 1–October 18, 2000). During this time, the changes of canopy height and plant green mass density are not so dynamic as at the start of the growing season (*Fig. 1*), and also their influence on the roughness length are minimal. The monthly average z_0-values were: $z_0 = 0.24$ m of the mean canopy height 2.24 m in August, $z_0 = 0.23$ m of $h = 2.20$ m in September, and $z_0 = 0.19$ m of $h = 2.15$ m in October. The roughness length of canopy surface is very often expressed as the fraction of the roughness elements height above the zero plane displacement, $(h - d)$. *Garratt* (1992) suggests that $z_0/(h - d)$ equals to 0.2–0.4. *Mölder* (1997) found for the barley field that $z_0 = 0.3(h - d)$. In our case, the monthly average values of $z_0/(h - d)$ for investigated maize stand equal to 0.32 in August and September, and 0.27 in October. This is well corresponded with the values found in literature.

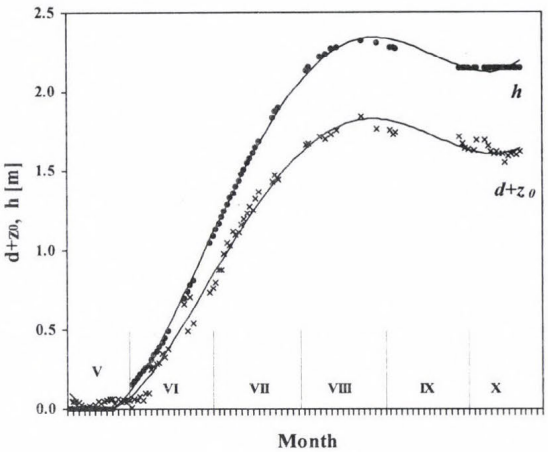

Fig. 1. Seasonal course of daily average values of canopy height h and $(d+z_0)$, where d is the zero plane displacement height and z_0 is the roughness length of the maize canopy.

At first the dependence of the friction velocity u^* on the wind speed measured at the level of plant height, $u(h) \sim u(0.5\ \text{m})$ at closed maize canopy, was analyzed. Assuming z_0 and d are constant with the wind speed, the linear equation, $u^* = Au(h)$, where A is constant, is followed from the log law. Then, as it was introduced by Hayashi, the canopy is in an aerodynamical steady state (*Hayashi,* 1983). In this case the z_0 and d values are not dependent on the wind speed. But for a real canopy, the friction velocity settles down and deviates from the linear equation. The u^* values were calculated from the wind speed profile analysis, Eq. (9). In our case, on the basis of the analyzed observations, the wanted function for investigated maize canopy during August 1–October 18, 2000 can be fitted as follows, $u^* = 0.62[u(0.5\text{m})]^{0.69}$ (*Fig. 2*). The correlation coefficient between u^* calculated by this equation and calculated from the wind speed profiles was 0.68. It is necessary to be aware, that u^* values depend not only on the wind speed but also on z_0. It may be an explanation for the dispersion of experimental points in *Fig. 2*. From this analysis it follows, that this closed maize canopy was in an aerodynamically variable state, and so the z_0 values will be dependent on the wind speed. The function $z_0 = \text{f}(u)$ can be analyzed as the dependence of the relative roughness length ξ_0 on the nondimensional speed Γ Then the dependence $\xi_0 = \text{f}(\Gamma)$ for investigated closed maize canopy from August 1 to October 18, 2000 can be expressed by analytical relationship in the form (*Fig. 3*):

$$\xi_0 = \frac{z_0}{h} = 0.162 \exp(-0.306\,\Gamma). \tag{12}$$

The correlation coefficient between z_0 calculated by Eq. (12) and calculated from the wind speed profiles was 0.96.

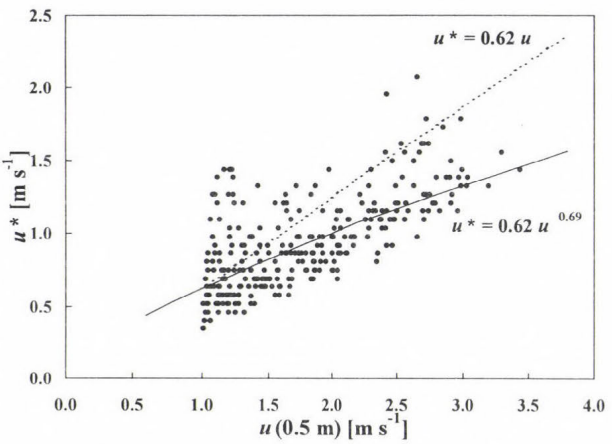

Fig. 2. Dependence of the friction velocity u^* on the wind speed $u(0.5\ \mathrm{m})$.

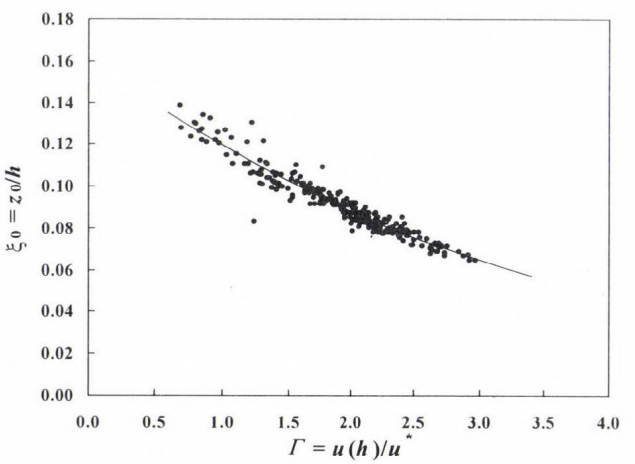

Fig. 3. Dependence of the relative roughness length ξ_0 on the nondimensional speed Γ for closed maize canopy.

From wind speed profile analysis also the r_a values were calculated using Eq. (11). The dependence of the r_a values on the wind speed $u(2\ \mathrm{m})$ above maize canopy during the whole growing season is shown in *Fig. 4*. The fitted line has the form of the 3-order polynomial with correlation coefficient 0.51.

During this period, the r_a values (daily averages) were from the interval 1.38–63.48 s m^{-1} (*Fig. 5*). Maximum value of aerodynamic resistance over closed

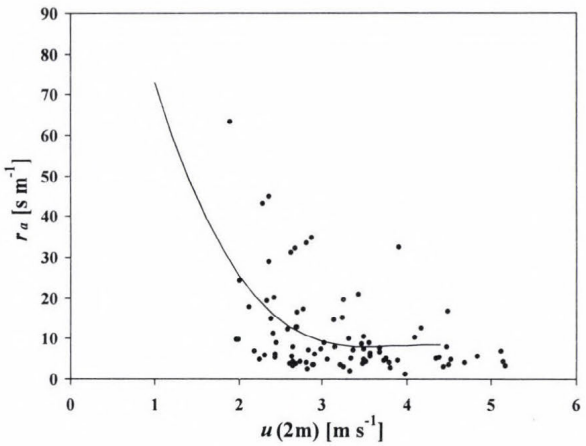

Fig. 4. Variation in the aerodynamic resistance r_a with the wind speed u(2 m) above maize canopy during the growing season.

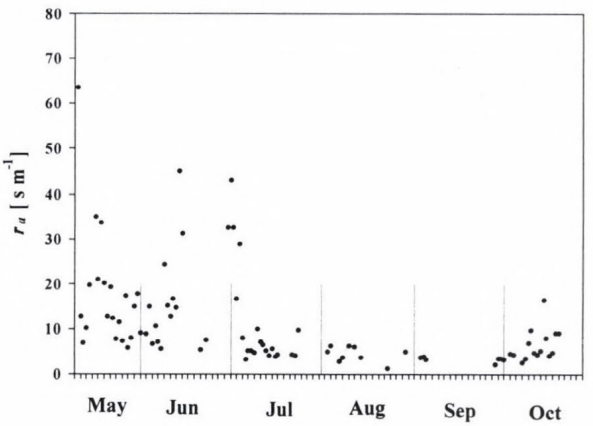

Fig. 5. Seasonal variations in the aerodynamic resistance r_a above maize canopy during the growing season.

canopy surface (August, September) was only 6.27 s m^{-1}. In October the r_a values were higher with maximal value of 16.52 s m^{-1}. As it was written before, the aerodynamic resistance also can represent the water vapor transfer through the canopy air and in the air above this canopy (*Brutsaert,* 1982;

Hurtalová, 1995). It may be seen, that the r_a values are high over bare soil (May) and above surface covered by canopy with low *LAI*-values (June), and they are low above closed canopy surface (August, September). In October, when *LAI* of the maize stand decreases, the r_a values have grown a little. Further it can be seen, that the aerodynamic resistance decreases with increasing wind speed. However, this dependence is more complicated, because the r_a values depend also on the roughness length and the atmosphere's thermal stratification. The experimental points dispersion in *Fig. 4* is the evidence of this fact. This is well in comformity with results found in literature (*Wallace et al.,* 1984).

5. Conclusion

The zero plane displacement, roughness length, and aerodynamic resistance values were determined during the whole maize growing season. The average roughness length of closed maize canopy was from 0.24 m in August to 0.19 m in October, with mean canopy height of 2.24 m and 2.15 m, respectively. The monthly average values of $z_0/(h - d)$ for closed maize canopy equaled to 0.32 of mean canopy height of 2.22 m. Further, the results showed that values of the roughness length determined for maize canopy during the whole growing season were practically independent of the mean height of this canopy. It has as a result that the often used estimation of the roughness lengths as $0.1h$ is not always appropriate.

This study confirms that aerodynamic properties of air layer above maize canopy surface vary with wind flowing. On the basis of the wind speed profile analysis it was found, that the dependence of friction velocity u^* on the wind speed $u(0.5\text{m})$ above investigated closed maize canopy was expressed by the relationship $u^* = 0.62[u(0.5\text{m})]^{0.69}$. It means, that maize canopy was in an aerodynamically variable state, and the roughness length values depend on the wind speed. Further it was shown, that Eq. (12) well approximates the changes of z_0 values of investigated maize canopy surface with the air flow.

The aerodynamic resistance decreases with increasing wind speed. This dependence is more complicated, because the r_a-values depend also on the rougness length and the atmosphere's thermal stratification. Maximum value of aerodynamic resistance over closed canopy surface (August, September) was only 6.27 s m^{-1}. In October the r_a values were higher with maximal value of 16.52 s m^{-1}.

Acknowledgements—The authors are grateful to the Slovak Grant Agency VEGA (Grant No 2/2093/22) and the Ministry of Education, Youth and Sports of Czech Republic (Grant No J08/98:432100001) for partially supporting this work.

References

Brutsaert, W.H., 1982: *Evaporation Into the Atmosphere.* D. Reidel Publishing Company, London.

Garratt, J.R., 1992: *The Atmospheric Boundary Layer.* Cambridge University Press, Cambridge.

Hayashi, Y., 1983: *Aerodynamical Properties of an Air Layer Affected by Vegetation. Environm. Res. Center Papers, 3.* ERC the University of Tsukuba, Ibaraki.

Hurtalová, T., 1995: Aerodynamic resistance role in plants-atmosphere system. *Contr. Geophys. Inst. SAS, Ser. Meteorol. 15*, 52-61.

Hurtalová, T., Janičkovičová, L., and *Matejka, F.*, 1987: Dynamic roughness - an aerodynamic characteristic of the active surface. *Contr. Geophys. Inst. SAS, Ser. Meteorol. 18*, 56-64.

Hurtalová, T. and *Matejka, F.*, 1999: Surface characteristics and energy fluxes above different plant canopies. *Agric. and Forest Meteorol. 98-99*, 491-500.

Hurtalová, T. and *Szabó, T.*, 1985: Die Abhängigkeit des Integralkoeffizienten der turbulenten Diffusion von ausgewählten meteorologischen Parametern. *Z. Meteorol. 35*, 354-358.

Jasinski, M.F. and *Crago, R.D.*, 1999: Estimation of vegetation aerodynamic roughness of natural regions using frontal area density determined from satellite. *Agric. and Forest Meteorol. 94*, 65-77.

Matejka, F., Hurtalová, T., Rožnovský, J., and *Chalupníková, B.*, 2001: Effect of soil drought on evapotranspiration of maize field. *Contrib. to Geophysics and Geodesy 31*, 455-466.

Monin, A.S. and *Obukhov, A.M.*, 1953: Dimensionless characteristics of turbulence in the atmospheric surface layer (in Russian). *Doklady AN SSSR 93*, 223-226.

Monin, A.S. and *Obukhov, A.M.*, 1954: Basic turbulent mixing law in the atmospheric surface layer (in Russian). *Trudy Geofiz. Inst. AN SSSR*, 24(151), 163-187.

Mölder, M., 1997: Parametrization of exchange processes over a barley field. *Boundary-Layer Meteorol. 84*, 341-361.

Mölder, M., Grelle, A., Lindroth, A., and *Halldin, S.*, 1999: Flux-profile relationships over a boreal forest - roughness sublayer corrections. *Agric. and Forest Meteorol. 98-99*, 645-658.

Rožnovský, J. and *Svoboda, J.*, 1995: Agroclimatological characteristics of Žabčice region (in Czech). *Folia, Series A.* Mendel Agricultural and Forestry University, Brno.

Rožnovský, J., Svoboda, J., Žalud, Z., and *Šťastná, M.*, 2000: Meteorological characteristics of dry spring 2000. In MZLU to Growers, Žabčice 2000. *Proc. of Contributions from Field Days.* MZLU in Brno, 72-75.

Saugier, B. and *Ripley, E.A.*, 1978: Evaluation of the aerodynamic method of determining fluxes over natural grassland. *Quart. J. Roy. Meteorol. Soc. 104*, 257-270.

Wallace, J.,S., Lloyd, C.,R., Roberts, J., and *Shuttleworth, W.,J.*, 1984: A comparison of methods for estimating aerodynamic resistance of heather in the field. *Agric. and Forest Meteorol. 32*, 289-305.

BOOK REVIEW

Wilfried Schröder (editor): **Meteorological and Geophysical Fluid Dynamics (A book to commemorate the centenary of the birth of Hans Ertel)**. Science Edition, D-28777 Bremen-Rönnebeck, 2004, 417 pages. Price: 20 EUR.

Professor Hans Richard Max Ertel was born in 1904 and died in 1971. He is a highly recognised scientist for his work related to geophysics, meteorology, and hydrodynamics. His earlier research covered a much wider range, it touched even the cosmology. The German Commission for the History of Geophysics and Cosmical Physics decided to collect into one volume tributes and greetings (25), as well as scientific papers (34) dedicated to Professor Ertel. The book contains the first and last papers written by himself, the greeted scientist.

The papers deal with every aspect of geophysics, the authors represent several countries as it can be expected in the case of a memorial book. This way the reader will have a possibility to be informed of several fraction of geophysics and hydrodynamics. It seems, Dr. Schröder's editorial work very well serves both: Professor Ertel's tribute and the readers interests.

G. Major

GUIDE FOR AUTHORS OF *IDŐJÁRÁS*

The purpose of the journal is to publish papers in any field of meteorology and atmosphere related scientific areas. These may be

- research papers on new results of scientific investigations,
- critical review articles summarizing the current state of art of a certain topic,
- short contributions dealing with a particular question.

Some issues contain "News" and "Book review", therefore, such contributions are also welcome. The papers must be in American English and should be checked by a native speaker if necessary.

Authors are requested to send their manuscripts to

Editor-in Chief of IDŐJÁRÁS

P.O. Box 39, H-1675 Budapest, Hungary

in three identical printed copies including all illustrations. Papers will then be reviewed normally by two independent referees, who remain unidentified for the author(s). The Editor-in-Chief will inform the author(s) whether or not the paper is acceptable for publication, and what modifications, if any, are necessary.

Please, follow the order given below when typing manuscripts.

Title part: should consist of the title, the name(s) of the author(s), their affiliation(s) including full postal and E-mail address(es). In case of more than one author, the corresponding author must be identified.

Abstract: should contain the purpose, the applied data and methods as well as the basic conclusion(s) of the paper.

Key-words: must be included (from 5 to 10) to help to classify the topic.

Text: has to be typed in double spacing with wide margins on one side of an A4 size white paper. Use of S.I. units are expected, and the use of negative exponent is preferred to fractional sign. Mathematical formulae are expected to be as simple as possible and numbered in parentheses at the right margin.

All publications cited in the text should be presented in a *list of references*, arranged in alphabetical order. For an article: name(s) of author(s) in Italics, year, title of article, name of journal, volume, number (the latter two in Italics) and pages. E.g., *Nathan, K.K.,* 1986: A note on the relationship between photo-synthetically active radiation and cloud amount. *Időjárás 90,* 10-13. For a book: name(s) of author(s), year, title of the book (all in Italics except the year), publisher and place of publication. E.g., *Junge, C. E.,* 1963: *Air Chemistry and Radioactivity*. Academic Press, New York and London. Reference in the text should contain the name(s) of the author(s) in Italics and year of publication. E.g., in the case of one author: *Miller* (1989); in the case of two authors: *Gamov* and *Cleveland* (1973); and if there are more than two authors: *Smith et al.* (1990). If the name of the author cannot be fitted into the text: *(Miller,* 1989); etc. When referring papers published in the same year by the same author, letters a, b, c, etc. should follow the year of publication.

Tables should be marked by Arabic numbers and printed in separate sheets with their numbers and legends given below them. Avoid too lengthy or complicated tables, or tables duplicating results given in other form in the manuscript (e.g., graphs)

Figures should also be marked with Arabic numbers and printed in black and white in camera-ready form in separate sheets with their numbers and captions given below them. Good quality laser printings are preferred.

The text should be submitted both in manuscript and in electronic form, the latter on diskette or in E-mail. Use standard 3.5" MS-DOS formatted diskette or CD for this purpose. MS Word format is preferred.

Reprints: authors receive 30 reprints free of charge. Additional reprints may be ordered at the authors' expense when sending back the proofs to the Editorial Office.

More information for authors is available: antal.e@met.hu

Information on the last issues: http://omsz.met.hu/irodalom/firat_ido/ido_hu.html

Published by the Hungarian Meteorological Service

Budapest, Hungary

INDEX: 26 361

HU ISSN 0324-6329